PCCP

PERSPECTIVE

View Article Online
View Journal | View Issue

Cite this: *Phys. Chem. Chem. Phys.*, 2023, **25**, 18623

First-principles design of nanostructured electrode materials for Na-ion batteries: challenges and perspectives

Arianna Massaro, *[ab] Francesca Fasulo, [bc] Adriana Pecoraro, [bc] Aniello Langella, [a] Ana B. Muñoz-García [bc] and Michele Pavone *[ab]

Received 16th March 2023,
Accepted 20th June 2023

DOI: 10.1039/d3cp01201h

rsc.li/pccp

Post-lithium batteries are emerging as viable solutions for sustainable energy transition. Effective deployment in the market calls for great research efforts in the identification of novel component materials and the assessment of related working principles. Computational modelling can be a key player in boosting innovation and development by enabling rational strategies for the design of appropriately tuned materials with optimized activity towards battery operating processes. By gaining access to the structural and electronic features of functional electrodes, state-of-the-art DFT methods can unveil the subtle structure–property relationship that affects the uptake, transport, and storage efficiency. Hereby, we aim at reviewing the research status of theoretical advances in the field of Na-ion batteries (NIBs) and illustrating to what extent atomistic insights into sodiation/desodiation mechanisms of nanostructured materials can assist the development of effective anodes and cathodes for stable and highly performing devices. Thanks to increasing computer power and fruitful cooperation between theory and experiments, the route for effective design methodologies is being paved and will feed the upcoming developments in NIB technology.

1. Introduction

The chance to enable reversible electrical-to-chemical energy conversion is powering the technological progress in a multitude of applications. Rechargeable batteries are among the most sought after electrical energy storage (EES) systems, with the pioneering Li-ion battery (LIB) technology reaching a huge technological and social impact, as evidenced by the recognition through the 2019 Nobel Prize in Chemistry.[1,2] Lately, the urgent need for a green economy is pushing the production of sustainable EES systems on a very large scale, and other applications than microelectronics have put battery research in the spotlight.[3] The scarce availability and the restricted geographical distribution of lithium and other typical LIB components (*e.g.*, cobalt) are expected to limit the large-scale integration of Li batteries in electric vehicles or stationary electrical grids.[4] Energy storage research is currently heading toward creating new options based on cheaper and widespread resources with the general goal of obtaining similar or better performances than state-of-the-art LIBs.[5] Thanks to easily available sodium raw materials, Na-ion batteries (NIBs) are among the most valid sustainable alternatives, and the similarities with LIBs have facilitated a rapid development of component materials starting from those already known.[6,7] However, most LIB components are not as effective as in Na-analogues: while the size of Na^+ helps the diffusion through liquid electrolytes, it hampers a convenient and reversible intercalation into the electrode structure.[7–10] The Li-to-Na replacement in many cathodes leads to extremely intertwined electrochemistry, involving unexpected phase transformations upon cycling, while Na^+ insertion into state-of-the-art graphitic materials results in largely unstable intercalated compounds.[7–10] Thus, the scientific community of chemists, physicists and materials scientists plays an active role in developing novel functional materials for highly performing NIB electrodes. Significant breakthrough has already been achieved by pursuing nano-engineering strategies to improve charge transfer kinetics at the electrode/electrolyte interface.[11,12] Lithium-to-sodium transition has been fed with dynamic research advances and fast progress in materials development. To commercialize NIBs as cost-efficient batteries based on abundant elements, specific advantages over LIBs should be attained in the near future in order to face the increasing demand in resource and chains supply. From a

[a] *Department of Chemical Sciences, Università di Napoli "Federico II", Compl. Univ. Monte Sant'Angelo, via Cintia 21, 80126, Napoli, Italy. E-mail: arianna.massaro@unina.it, michele.pavone@unina.it*
[b] *National Reference Centre for Electrochemical Energy Storage (GISEL) - INSTM, 50121 Florence, Italy*
[c] *Department of Physics "E. Pancini", Università di Napoli "Federico II", Compl. Univ. Monte Sant'Angelo, via Cintia 21, 80126, Napoli, Italy*

scientific and chemical point of view, investigating the efficiency of host electrode materials toward Na uptake and storage and the electrochemical stability of Na conductive electrolyte systems will represent the main contribution. Many challenges that were not conceived for LIBs are actually present for NIBs and should be addressed with the aim of creating new options for future energy storage devices, and this also includes the use of Na in solid-state, metal/air- and metal/sulphur-batteries.

The identification of novel materials and an in-depth comprehension of their electrochemical behaviour are crucial steps in the whole production process prior to the ultimate application in real devices. Electrochemical reactions within batteries are complex phenomena, often including undesired and even detrimental processes that determine the overall system performance. In this context, computer-aided design can be extremely beneficial for spanning the atomic-to-macro length scales in order to understand the intertwined physico-chemical processes at play and to gain the desired improvement in stability and performance. With this purpose, computational approaches are widely applied to other energy storage technologies relying on different materials or working processes. The promising Na–S and Na–O_2 batteries rely on conversion reactions at the sulphur–carbon composite or oxygen-exposed porous electrode, respectively (*i.e.*, positive electrodes) led by Na ions deriving from Na metal oxidation (*i.e.*, negative electrode). By addressing the stability of common discharge products (short- or long-chain sodium polysulfides, Na_2S_x, or sodium oxide, superoxide, and peroxide, Na_2O, NaO_2 and Na_2O_2, respectively), and the related feasible reactivity with electrolyte components, first-principles calculations have elucidated the main structure–properties relationship undermining the overall cell capacity and delivered new insights into how to improve shuttle effects, slow kinetics and poor electron conductivity.[13–17]

At the foundation of any computational approach there are quantum-mechanics (QM) methods that can access the electronic structure of materials and the mechanistic details of sodiation/desodiation at the nanoscale, allowing for a fundamental understanding of redox reactions, ion diffusion, as well as the role of defects along the charging/discharging process.[18–21] Advanced electronic structure calculations generally require *ab initio* techniques and the solution of the appropriate Hartree–Fock equation, which is demanding and usually limits the system size. For most problems, density functional theory (DFT) serves the same purpose with lower computational costs. On the other hand, meso-to-macroscopic scale-based phenomena, such as dendritic growth, microstructuring, or degradation processes, can be addressed *via* molecular mechanics methods, including force-field and coarse-graining techniques.[22–26] Notwithstanding the great advances and the broad literature, major efforts are still required to attain full knowledge of either the component material itself or the heterogeneous electrode/electrolyte interface, where complex charge transfer processes take place during battery functioning. With the advent of multiscale modelling, resolving questions over several length and time scales or exploring how microscopic and macroscopic phenomena are interrelated is rapidly emerging.[27] The idea of combining atomistic and macroscopic simulations into a multiscale perspective is at the forefront of theoretical investigations in many fields and will drive the upcoming challenges towards realistic modelling of battery materials and their behaviours. Developing sophisticated force fields able to reproduce charge polarization effects, complex reaction pathways and interfacial structuring and dynamics, have the potential to solve generality, accuracy, and reliability issues.[28–33] More recently, Machine Learning potentials trained on QM reference data have offered a valuable alternative to classical interatomic potential fitting, and can be used to explore the associated energy surfaces with comparable accuracy.[34–37]

The upsurging interest for computational-driven design in the energy storage field can be effectively demonstrated by the increasing number of related publications. Many recent reviews discuss the great challenges that the theoretical chemistry community is currently facing, ranging from the importance of preliminary method validation,[38] to the key role of dynamic features and ionic conductivity in assessing both electrode and electrolyte development,[39,40] as well as the fundamental understanding of electrode–electrolyte complex interfaces, especially for future exploitation of all-solid-state-batteries.[41] Whether setting foundations for advancing in multiscale techniques or delivering fundamental knowledge on electroactive materials, QM-based simulations still represent the driving force towards rational design and offer solid and reliable grounds for investigating reaction kinetics, electrochemical potentials, chemical stability, defects chemistry, and adsorption/dissociation energetics.

In this perspective, we provide an overview of recent works from our laboratory on nanostructured electrode materials addressed by first-principles methods. With these examples we offer a general view on the subtle structure–property-function relationships that directly affect the main processes related to battery functioning and that can be exploited to derive original design principles. Provided that appropriate methods must be considered to face specific theoretical challenges, the application of the DFT framework is proven to offer suitable tools for a large variety of material families. The optimal accuracy/computational cost ratio can be achieved by employing the DFT+U scheme to tightly localized d-electrons (*e.g.*, transition metal oxides, U_{eff} = 3.3 eV for Ti and U_{eff} = 4.0 eV for Mn, Ni, Fe and Ru, see Sections 2.1 and 3, respectively) in order to correct the large self-interaction error (SIE),[42–45] or the *a posteriori* DFT-D correction to account for key van der Waals (vdW) interactions in interfaces (Section 2.1) and layered structures (Section 3).[46–49] Application of DFT-based state-of-the-art computational protocols is shown to provide insightful details on relevant topics: Na^+ intercalation in nanostructured anodes and the related effects of morphology and external electric field (Section 2); charge compensation in high-energy cathodes and the tuneable activation of reversible anionic oxygen redox chemistry (Section 3). By performing spin-polarized DFT-PBE calculations within the generalized gradient approximation (GGA) with projector-augmented wave (PAW) potentials and plane wave (PW) basis sets,[50,51] reliable models for solid-state crystalline nanoelectrodes can be obtained with affordable computational efforts (forces accuracy for geometry relaxation: 0.03 eV $Å^{-1}$; energy

accuracy: 10^{-5} eV). Kinetic energy cutoff and *k*-points sampling schemes are determined *via* convergence tests to ensure converged energies within 3 meV f.u.$^{-1}$. Dipole corrections are applied to slab models when considering surface structures so as to avoid long-range polarization from the periodic images along the *c*-direction (see Sections 2.1 and 2.2).[52] By deriving readily computable descriptors that can be directly compared to experimental data, the reported case studies shed light on the electrochemical behaviour of promising NIB systems and drive future strategies for effective tuning of functional materials.

2. NIB anodes: hybrid and nanostructured materials

In the development of solid-state anodes for Na-ion batteries, the most important requirement is represented by the crystalline structure and its mechanical response to a significant stress, *i.e.*, the Na^+ intercalation. The lattice should feature suitable host sites for the large Na^+, and the crystalline network must be robust enough to retain its shape upon subsequent Na^+ insertion/extraction.[53] Anode materials should also exhibit oxidation potentials as close as possible to 0 V *vs.* Na^+/Na. In view of developing high energy density batteries, materials research is confined to those families of negative electrodes which allow sodiation/desodiation at few tenths of volts *vs.* Na^+/Na (*e.g.*, carbon-based materials, metal oxides, alloys).[11,54–56] However, the operation of most negative electrodes in the low voltage range may be coupled to electrolyte decomposition and metal plating, disturbing both cycle life and safety. Development of highly stable and durable anode materials usually calls for the need of functionally engineered and protective Solid Electrolyte Interphase (SEI) layers.[57,58] The scientific literature in this field has been recently enriched with computational modelling and insights from *ab initio* simulations. The large variety of proposed materials basically differ for the sodiation/desodiation mechanism. Whether they undergo insertion, conversion, or intercalation processes, the atomistic perspective can supply reliable and affordable models to describe the underlying mechanisms and understand the crucial features. From a general perspective, the anodes exploration is mainly motivated by the ineffective intercalation of Na^+ into state-of-the-art graphite, which has led to a broad range of systems, including carbonaceous materials, Na-binary alloys, or conversion reaction anodes. As the limiting factor for the unfavourable intercalation, the weak Na-graphite binding can be effectively overcome by ensuring larger interlayer spacing in hard or soft carbons,[59] but also *via* introduction of various point defects into carbon scaffolds, such as mono-vacancy, divacancy, and Stone–Wales defects.[60] The first-principles predictions of voltage profiles and structural evolution upon sodiation have enabled the screening of promising Na-binary alloys with both Group-14 and Group-15 element compounds, such as c-Na_xSn, a-Na_xGe, a-Na_xSi and Na–P species.[61,62] By unveiling complex reaction pathways, computational studies have also assisted the development of tricky M_aX_b phases (M = Sn, Sb; X = O, S, Se). While allowing high specific capacity, these materials usually undergo severe volume expansion upon cycling which still limits their practical applications.[53] Recently, hybrid and nanostructured materials have attracted increasing consideration as NIB anode applications owing to tuneable shape, morphology and composition that can give the electrodes boosted sodium storage performance. In the following, we present a few representative studies on emerging anode materials, which have recently exemplified the key role of computational-driven design.

2.1 Sodiation process in intercalation anodes: the key role of migration mechanisms

Na^+ uptake and storage at the anode interface can occur *via* adsorption of a Na cation on the surface, followed by its migration through the lattice. Thus, the adsorption energy can be easily calculated as:

$$E_{ads} = E^{OUT}_{Na@host} - E_{host} - E_{Na} \quad (1)$$

where $E^{OUT}_{Na@host}$ and E_{host} are the total energies of the Na-electrode system and the electrode itself, respectively, and E_{Na} is the total energy of one sodium atom inside the Na metal bcc unit cell, that is used as reference.[63] In principle, it is possible to distinguish several Na–host interacting sites. If the process takes place in the lattice subsurface, the inserted Na–host system will define an insertion energy, E_{ins}, as follows:

$$E_{ins} = E^{IN}_{Na@host} - E_{host} - E_{Na} \quad (2)$$

Adsorbed or inserted configurations represent a suitable model for initial considerations about the bare Na–electrode interactions and the related n-type contact which can be unveiled from electronic structure analysis. However, it turns out to be ineffective for reliable predictions about the electrochemical behaviour. This is because the sodiation performance cannot neglect the storage step, *i.e.*, migration. Once the Na atom is adsorbed on the electrode surface, it can move through the lattice across a diffusion channel and eventually reach inserted or other possible adsorption sites. By means of the climbing-image nudged elastic band (CI-NEB) approach, it is possible to identify the minimum-energy pathways across different equilibrium structures (*i.e.*, the Na adsorbed/inserted sites) through high-energy transition states, identified as saddle points of the potential energy surface.[64] The corresponding barrier heights are derived as:

$$E_{migr} = E_{Na^{TS}} - E^{OUT/IN}_{Na@host} \quad (3)$$

where $E_{Na^{TS}}$ and $E^{OUT/IN}_{Na@host}$ are the total energies of the Na–electrode system at the transition state along the migration coordinate and its adsorbed/inserted state described before (see eqn (1) and (2)). In this way, the OUT/IN migration can be evaluated separately. This represents a common theoretical framework built for *ab initio* investigations on NIB anodes and related Na^+ intercalation and migration mechanisms.

In the context of NIB anodes, many research efforts are focused on the applications of carbonaceous materials as

sustainable and electroactive systems. Given the successful employment of graphite anodes in LIBs, great attention has been paid to disordered hard carbons or graphite-like soft carbons, exposing a porous surface area with a more appropriate layered structure for Na^+ uptake and storage.[65] The reported sodiation activity is generally good, but some improving strategies can be pointed out thanks to first-principles studies. For example, Tsai *et al.* have highlighted the role of vacancy defects in favouring the Na intercalation capability thanks to the enhanced Na^+-vacancy ionic binding interactions.[60] Alloy formation represents another possible route, especially when enabled by the use of low-cost silicon-based materials exhibiting very high specific capacity (954 mA h g^{-1}).[66] Huge volume variations usually represent the main drawbacks, but they are minimized in an Na_xSi_{24} allotrope that cycles in a single-phase regime without any nucleation, as unveiled from DFT investigations.[67] Migration analysis performed with CI-NEB has also identified the constrained relaxation of the eight-member silicon ring as the limiting factor in Na mobility when moving from a dilute to concentrated regime.[67] Few works are also dedicated to germanium based alloys, where *ab initio* molecular dynamics simulations have reported the full amorphization occurring after earlier Na clustering at low sodiation as the main driving force for enhanced diffusivity compared to crystalline samples.[68] With silicon-based materials often suffering from unbearable volume change, a combination with more robust C-based materials has appeared as a promising solution. Sodium migration along the *z*-direction in silicon–carbide (Si–C) exhibits a minimum energy barrier compared to other lattice directions, which can be further lowered *via* vacancy introduction.[69] As reported by Dhillon *et al.*, numerical simulations can also be insightful: the capacity fading in silicon–graphite composite electrodes seems to be induced more by Si cracking upon cycling rather than the SEI layer growth, and this effect can be prevented by varying the ratio of graphite and silicon accordingly.[70] Application of C-based materials is also key in organic batteries, where DFT methods have been applied to predict crystalline structures or redox mechanistic details.[71] Graphene also represents a highly pursued material in the battery field, especially in combination with other systems, as electron buffer and robust mechanical support.[72] Creating hybrid interfaces to 2D transition metal dichalcogenides (TMDCs) with tuneable interlayer spacing could provide the anode material with the desired intercalation structure for Na ions.[73] Fabrication of MoS_2/graphene anodes *via* easy and low-cost processes has led to high-quality and efficient materials, but dissecting the role of each component or the interface still represents a crucial point.[55,74] Wang *et al.* showed how interconnected 3D carbon networks in MoS_2/C superstructures are responsible for improving electron transport and Na^+ diffusion, while retarding the volumetric strain effect of MoS_2.[75] In a recent study from our group, we addressed the effects of MoS_2 phases on Na intercalation and migration properties.[76] Our dispersion-corrected DFT analysis showed that both 3R- and 1T-MoS_2/graphene result in electronically conductive heterostructures featuring a graphene-to-MoS_2 charge transfer, which would make the MoS_2 more prone to interact with the intercalating Na ion.[76] Among the multitude of intercalation sites, the overall adsorption energies suggest stronger Na–MoS_2 interaction for the 1T case, which correlates with the increased stability of this phase when exfoliated in the presence of alkali metals.[77] By considering migration pathways within the interlayer spacing, Na can move along the *x* direction, where the S atoms pointing toward the interlayer spacing seem to form an appropriate diffusion channel, with the reaction coordinate being the Na–Na distance after each Na jump, *i.e.*, ξ (see Fig. 1). Sodium migration in MoS_2/graphene heterostructures has been extensively addressed, either in bulk or freestanding MoS_2, graphene sheets, as well as on graphene-supported MoS_2 monolayers.[78–82] Our results allowed us to conclude that the interlayer mechanism exhibits the lowest barrier, thus representing the more convenient option for Na mobility (from our results: $E_{migr} \sim 0.17$–0.22 eV for 3R-MoS_2/graphene and ~ 0.08 to ~ 0.70 eV for 1T-MoS_2/graphene, calculated according to eqn (3)). The diffusion mechanism has been also coupled to the enlargement of the interlayer spacing occurring upon Na^+ passage from the minimum- to the highest-energy structure, and the effect is more relevant in the 1T phase (*i.e.*, from 3.11 Å to 3.70 Å, *vs.* from 3.35 Å to 3.76 Å in the 3R phase).

In the development of 2D-hybrid systems, understanding the role of possible polymorphs, interlayer spacing or interfacial features in determining the overall electrochemical performance of MoS_2/graphene-based electrodes can be crucial. With migration mechanisms at the 2D heterojunction being unveiled from first principles, experimental works can set up specific synthesis pathways (*e.g.*, phase-selected and defects-engineering syntheses) and preparation procedures (*e.g.*, interlayer expanded interfaces) toward more functional products.[83–85]

Titanium oxides are also capable of reversibly intercalating Na at low redox potentials. Starting from the structural lithium analogue, the rock salt-type $Na_2Ti_3O_7$ has been proposed as NIB anode.[86] Computational studies have compared $Li_2Ti_3O_7$ and $Na_2Ti_3O_7$ performances in terms of lattice evolution upon lithiation/sodiation. The difference in intercalation potentials (~ 0.7 V) can be ascribed to different ionic sizes and polarizing features, leading to different stabilization or volumetric effects.[87] Still, the self-discharge phenomena observed for $Na_2Ti_3O_7$-based devices has been attributed to a large electrostatic repulsion computed for the discharged state, *i.e.*, $Na_4Ti_3O_7$, leading to structural instability and an increase in the Gibbs free energy.[88] TiO_2 is a versatile functional material with several applications, ranging from solar cells to photocatalysis and batteries. In the form of anatase, TiO_2 shows comparable performances to graphitic materials in LIBs, such as high reversible theoretical capacity (335 mA h g^{-1}), low volume variation upon cycling (less than 4%), and improved safety thanks to the structural robustness and high working potential.[89] However, the performances of anatase nanoparticles (NPs) as negative electrodes in NIBs seem to depend on the exposed surfaces, the (100) and (001) facets being much more effective than the most stable (101) surface.[54] Yang *et al.* have tried to explain the surface-dependent activities by means of bare adsorption properties, but the predicted trend did not match the observed activities.[90] The simple Na–TiO_2 coverage is not a complete nor reliable model for this kind of interface, where each

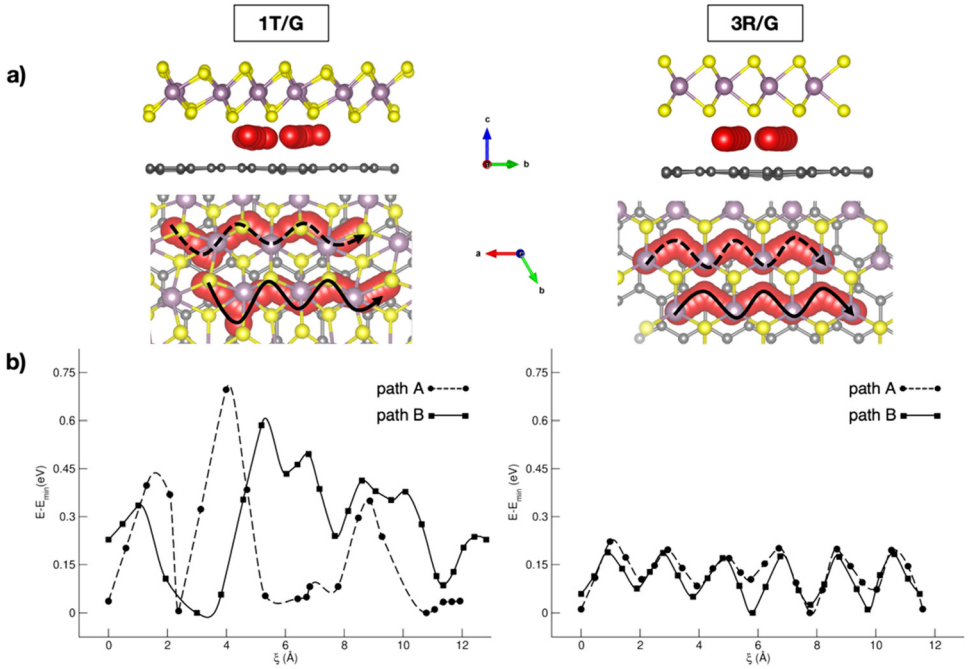

Fig. 1 (a) Side and top views of Na migration pathways through 1T- and 3R-MoS_2/G interfaces; (b) corresponding energetics computed with the CI-NEB method at the PBE-D3BJ level of theory. Reproduced from ref. 76 [A. Massaro *et al.*, *J. Phys. Chem. C*, 2021, **125**, 2276–2286]. Copyright 2021 American Chemical Society.[76]

surface acts as a Na^+ insertion site exhibiting pseudocapacitive behaviour.[54] In a recent work by our group, Na^+ insertion through the (101), (100) and (001) TiO_2 anatase surfaces has been addressed to prove the mechanism and the origin of observed selectivity toward Na^+ uptake.[91] Sodium migration can be defined as occurring between adsorption sites lying on top of surfaces and insertion sites in the subsurface layer along the [010] Na^+ diffusion channel (see Fig. 2).[92] The spatial coordinate along a migration pathway, ξ, is given by the Na–Na distance between two contiguous points acting as possible interstitial sites for ion accommodation and lying along suitable-sized diffusion channels. Sodium moves along a given direction in the lattice, passes across the alternating Ti–O motif, and then enters the cavity in the subsurface along the [010] diffusion channel. Migration analysis derived by the CI-NEB approach revealed that the (001) surface exhibits the lowest energy barrier in both forward and backward directions (*i.e.*, OUT/IN E_{migr}, calculated according to eqn (3)), suggesting that Na migration will be more likely to occur at this termination compared to (100) and (101).

The need for morphology-controlled production of TiO_2-based electrodes was already established in recent literature,[54,90,92] and is still feeding this research topic.[93] Having reliable surface models to describe sodiation at anatase interfaces is essential to provide insightful details on possible elements (*e.g.*, exposed surfaces, contact area, point defects) that may affect the Na^+ storage mechanism.

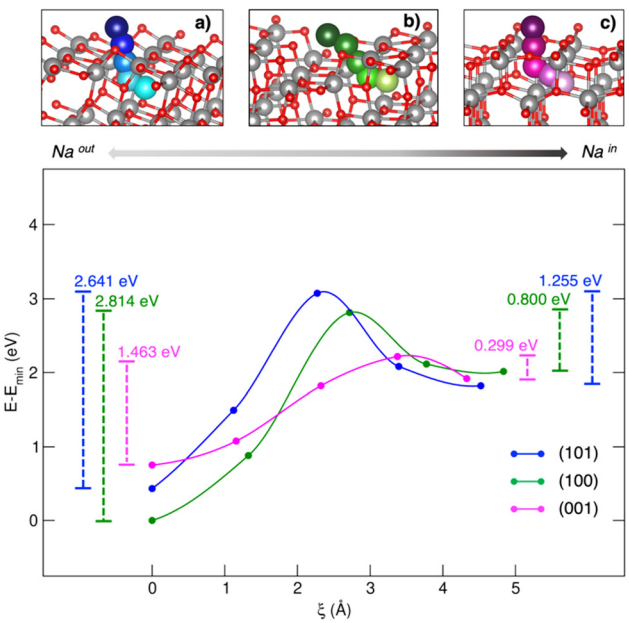

Fig. 2 Minimum energy paths (top) and corresponding energetics (bottom) for Na migration through the (a) (101)-, (b) (100)- and (c) (001)-TiO_2 anatase surfaces. Energy barriers calculated from eqn (3) for the out/in migration are reported, respectively, at the left- and right-hand sides of the graph. Reproduced from ref. 91 [A. Massaro *et al.*, *Nanoscale Adv.*, 2020, **2**, 2745] with permission from the Royal Society of Chemistry.[91]

2.2 New frontiers towards realistic simulations: the effects of an applied electric field

The studies reviewed so far highlighted the key role of theory in unveiling determining factors towards sodiation mechanisms of nanostructured anode materials. However, achieving accurate predictions by means of reliable models still represents a major challenge in computational chemistry applied to energy

storage. On one hand, simple models allow to gain interesting insights with little computational efforts, but they might be too far from the real device and other relevant information may not be detected. One example is given by the description of the sodiation process under electric field control. The battery operation takes place in a certain voltage range, under the passage of an electric current. A realistic model should therefore not neglect the effect of an electric bias applied to the materials under investigation, in order to overcome possible misinterpretations of thermodynamics and kinetics predicted by conventional DFT approaches encompassing 0-K, in-vacuum and equilibrium conditions. Although many field-related properties, including contact potentials or interfacial electric fields across SEI films, would require the quantitative application of such pioneering methodologies, the qualitative association of field polarization to specific processes can already provide new insights and pave innovative routes into this fundamental research area.[94,95] In this context, we have addressed the electric field effects on Na intercalation energetics as well as on structural and electronic properties of anatase surfaces.[96] The electric field is simulated in the direction perpendicular to the surface models by adding a sawtooth-like electrostatic potential to the bare ionic potential.[97] Positive and negative polarization can be considered, depending on whether the field lies in the same or opposite direction of the *z*-axis, thus giving a positive or negative slope, respectively. As illustrated in Fig. 3, insertion energies are essentially unchanged with the applied field, and minor structural modifications may be due to the high screening effects exerted by the surface layer. However, the field polarization does affect adsorption values and alters the IN–OUT gap. In particular, the positive field enlarges the energy gap for all the explored surfaces, while the negative one results in smaller differences (blue and red lines, respectively, in Fig. 3). Positive/negative directions lead to opposite effects, stabilizing the Na^{OUT} sites further/closer to the surface and promoting the oxidation/reduction of Ti sublattice.[96] Field polarization can therefore be thought as the bias direction that is present during battery cycling and accounts for the desodiation/sodiation of the anodic electrode upon discharge/charge (*e.g.*, the negative one favouring Na intercalation and leading to the reduction of Ti sublattice is representative of sodiation reaction upon charging). Thanks to the inclusion of electric field effects into DFT simulations, the theoretical investigations on electrode interfaces can make significant steps forward in modelling *in operando* conditions, thus improving the current understanding of electrochemical reactions at NIB electrodes.

The screening and predictive power of computational modelling can lead to high-impact outcomes that can drive the rational design of efficient materials. For example, further analysis performed in these case studies reveals that the Na storage activity in MoS_2/graphene heterostructures and TiO_2 anatase nanoparticles is ascribed to the intrinsic structural features of the electrodes. Na^+ migration barriers at the MoS_2/graphene interlayer spacing are associated to variations in the Na–S coordination when the transition state is reached, the effect being more relevant for the 1T phase compared to the 3R counterpart.[76] The single jump is more likely to occur when Na is further from sulphur atoms, thus the local structuring affects the sodium diffusion mechanism. Introducing S vacancies or tuning and nanoengineering the morphology of the MoS_2 phase can lead to promising design strategies aiming to reduce the Na–S hindering effects and enhance the overall mobility. Still, structural modifications occurring in the anatase surfaces upon Na migration can account for the different activities.[91] The size of the surface lattice window, *i.e.*, the minimum accessible area that Na^+ should cross to enter the TiO_2 crystalline structure, at the transition state (Na^{TS}), provides a direct measure of the steric hindrance that the migrating Na encounters along its path. This quantity can be calculated straightforwardly from the shortest Ti–Ti distance at the transition state structure (Na^{TS}).[91] Defined this way, this descriptor inversely correlates with the barrier heights: the largest lattice window is associated to the lowest migration barrier for the (001) surface (see Table 1). As a matter of fact, the surface lattice

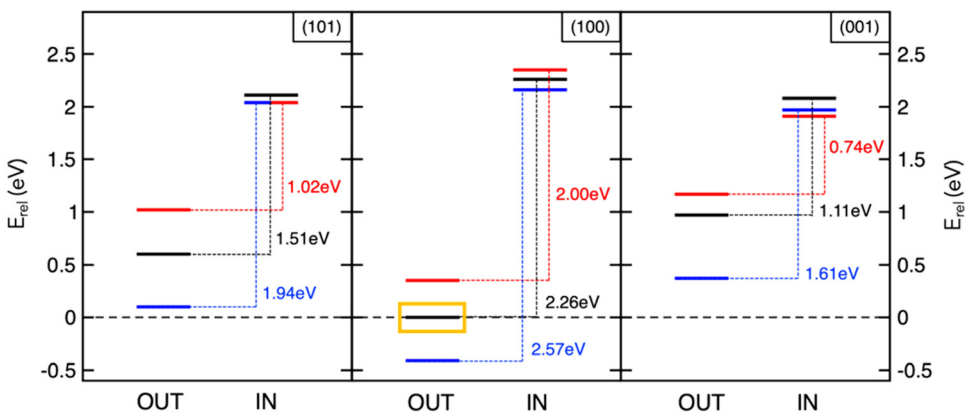

Fig. 3 Insertion and adsorption energetics for Na^{IN} and Na^{OUT} states at TiO_2 surfaces calculated at the PBE+*U* level of theory. All the energy values, E_{rel}, refer to Na-adsorbed on the (100) surface with zero-field (yellow box). Colour code: zero-field (black lines), positive field, $\vec{F} \times 10^3$ = 5 Ha (blue lines), and negative field, $\vec{F} \times 10^3$ = −5 Ha (red lines). Reproduced from ref. 96 [F. Fasulo *et al.*, *J. Mater. Res.*, 2022, **37**, 3216–3226]. Copyright © 2022, The Authors.[96]

Table 1 Minimum accessible areas (a_{min}) of the lattice windows calculated at zero-, positive and negative fields for (101)-, (100)-, and (001)-TiO_2 anatase surface terminations. The listed values are expressed in Å^2

System	a_{min} (zero-field)	a_{min} ($\vec{F} \times 10^3 = 5$ Ha)	a_{min} ($\vec{F} \times 10^3 = -5$ Ha)
(101)-TiO_2	8.60	8.58	8.64
(100)-TiO_2	8.71	8.68	8.73
(001)-TiO_2	15.14	14.83	15.14

windows get larger upon the effect of the negative field. Preferential use of (001)-containing NPs can be exploited to develop more efficient anatase-based NIB devices.

Notwithstanding these insightful outcomes, the rational design of efficient electrodes should not disregard the role of interfaces and the underlying processes: from charge transfer to migration/diffusion properties and interphase formation, up to the interfacial stability over the entire battery lifetime. It is widely recognized that almost all fundamental properties cannot be ascribed to the sum of the single components. Today, the interest in interface studies is rising from both theoretical and experimental communities, as established by an increasing number of scientific reports.[95,98] However, major computational challenges still need to be confronted to gain a full description of interfacial processes that usually occur across multiple lengths/timescales.[57,99] Herein, we have reported a preliminary attempt to include electric fields into the simulation environment, which would represent a viable way to consider more realistic electrochemical interfaces and the underlying modifications under electric field control.[96] The development of a unified workflow that intimately combines different techniques will be critical to enable this paradigm shift in battery design.

3. NIB cathodes: high-energy layered oxides

The development of high-energy, cheap, and structurally stable NIB positive electrodes operating at voltage values in the order of 4.5 V (or even above) represents a *Grand Challenge* because it is the cathode that mainly affects the battery performance and manufacturing costs. Polyanion materials, organic compounds and layered oxides undoubtedly represent the mostly investigated systems, whose peculiar features responsible for Na ordering, diffusion, and phase transformation, have been recently addressed and unveiled by computational studies. The *ab initio* determination of Na migration channels and the effect of antisite defects has enabled the optimization of efficient Na_xFePO_4 and Na_xMnPO_4 olivine structures.[100,101] By means of GGA+*U* methods, incorporation of highly electronegative F ions into phosphate-based materials has been shown to enhance the cathode voltage, and also lead to a robust crystalline lattice with facile 2D Na diffusion pathways.[102] Pioneering AIMD and NEB simulations on V-based fluorophosphates have then unveiled the interplay of Na and anion sublattice disordering as well as TM mixing to facilitate Na diffusivity within $Na_3V_2(PO_4)_2F_3$ (NVPF) systems.[103,104] Recent works have been devoted to heavy metal-free organic compounds, which would meet sustainability and environmental friendliness requirements. Theoretical challenges in the investigation of these materials (*i.e.*, disodium rhodizonate, benzoquinone derivatives, polyaniline (PANI), and tetracyanoethylene (TCNE)) include the subtle atomistic structure predictions.[105–107] The emergence of layered transition-metal oxides, Na_xTMO_2 ($0 < x < 1$), dates to the wide employment of $LiCoO_2$ in pioneering LIB prototypes.[108] However, the simple replacement with $NaCoO_2$ is impracticable due to critical phase transformations occurring upon desodiation, and the replacement with Mn- or Fe-based compounds also occurred for sustainability purposes.[109,110] The strong synergy of computational work with experimental studies drives major advances in the design of layered oxides as high-energy NIB cathodes, aiming to explore new classes of functional compounds while gaining a fundamental understanding that underpins applied research.[111]

As in Li counterparts, the crystalline structure of Na_xTMO_2 alternates planar layers of alkali metal ions and edge-sharing TMO_6 octahedra, where Na ions can easily move in and out upon cycling.[112] Among many polymorphs differing for stacking and internal symmetry, P2 and O3 (prismatic/octahedral sites for Na ions and 2/3 TMO_2-layers in the unit cell) phases are the most interesting for battery applications, showing different specific capacities, structural stability, and rate performances.[113] The charge/discharge operation can be considered as the shuttling of a certain fraction of Na ions, the driving force being the difference in the sodium chemical potential in the two electrodes. During discharge, the cathode material (low sodium chemical potential) is electrochemically reduced by intercalating Na^+ from the electrolyte and taking up electrons from an external circuit; simultaneously, the anode material (high sodium chemical potential) is oxidised. The overall reaction for a cell comprising a sodium transition-metal oxide intercalation cathode with Na_xTMO_2 composition and a Na metal anode would be:

$$Na_{x_1}TMO_2 \rightleftarrows Na_{x_2}TMO_2 + (x_1 - x_2)Na \quad (4)$$

The average voltage associated with eqn (4) arises from the Nernst equation as a function of the free energy change of the combined anode/cathode reaction. However, at low temperatures, entropic contributions can be neglected, and the $\Delta G_r \approx \Delta E_r$ approximation holds. The reaction free energy can be suitably quantified as the internal energy change, which can be obtained from independent first principles calculations for each system, and the Na chemical potential is conventionally approximated by the total energy of Na metal (*i.e.*, the reference electrode, that is the bcc crystalline phase).[114] Considering eqn (4) as a single step along the cathode charge, one can model different Na-containing structures as representing each state of charge. Thus, the whole sodiation range is covered, and the intercalation potential at each stage can be calculated as:

$$V = -\frac{E_{Na_{x_1}TMO_2} - E_{Na_{x_2}TMO_2} - (x_1 - x_2)E_{Na}}{(x_1 - x_2)} \quad (5)$$

where $E_{Na_{x_2}TMO_2}$ and $E_{Na_{x_1}TMO_2}$ are the total energies of $Na_\chi TMO_2$ at, respectively, x_2 and x_1 Na composition ($x_1 > x_2$), and E_{Na} is the total energy of one sodium atom inside the Na metal bcc unit cell.[63] The ratio and chemical nature of TM composition sensibly affect the phase stability and structural retention during subsequent Na insertion/extraction from the layered lattice.[110]

3.1 Charge compensation mechanisms upon desodiation unveiled from first principles

The electrochemical behaviour also depends on the involved TM redox couples, as the cathode sodiation/desodiation is compensated by the reversible reduction/oxidation of TM ions. How the chemical composition at the TM site determines the physical-chemical properties as well as the electrochemical response is decisive for the performance, but very challenging to predict.[115] Great efforts can be found in recent literature, where computationally derived descriptors serve as useful tools to predict the main properties from the chemical structure. One example is the cationic potential postulated by Zhao *et al.*, able to capture the key interactions of layered materials and make it possible to predict the stacking structures and the functional properties.[116] By employing DFT calculations to derive the average voltage, volume change and Na ion mobility, the screening method developed by Zhang *et al.* demonstrates how most promising candidates can be selected from the materials project database.[117] The vital role of theoretical investigations is also attested by the new insights gained in understanding the anionic redox activity, *i.e.*, the charge being stored not only by the TM cations but also by the oxide sublattice. This represents a new highly pursued paradigm for research and development of advanced cathode materials, pushing the theoretical specific capacity beyond the fixed limits of TM redox potentials. Whether anionic-redox active materials can accomplish a fully reversible process or undergo O_2 loss remains an open question. Which factors can drive the stabilization of oxygen electron holes and preserve the reversible activity upon subsequent cycling? In many Li-rich oxides with O3 stacking, O_2 release has often been associated with TM migration from the TMO_2 layer to the alkali metal one. DFT calculations performed by Wang *et al.* have shown that this kind of interlayer migration can safely be excluded in the O3-$NaLi_{1/3}Mn_{2/3}O_2$ phase.[118] While Mn cations are greatly stabilized in the interlayer space of pure-Li phases, the presence of Na^+ in the alkali layer imposes a too large c parameter, and Mn migration from the metallic to the alkali layer is therefore less favoured. Li^+ displacement towards the alkali layer upon first Na^+ deinsertion promotes the switching from inter- to intra-layer migration of Mn cations, preventing any voltage fade.[118] Anionic redox mechanisms can be intertwined, especially when electrochemical cycling leads to phase transformation. Vergnet *et al.* have unveiled the voltage hysteresis of $Na_xMg_{1/3}Mn_{2/3}O_2$ from first principles, by revealing the competition between a reductive coupling mechanism occurring in P stacking, which is quite reversible, and a disproportionation of oxygen network into peroxo-like pairs and oxo-like atoms in the O stacking, inducing migrations that facilitate oxygen release and entail structural instability.[119] The first-cycle voltage hysteresis has also been associated to superstructural ordering in $Na_{0.75}[Li_{0.25}Mn_{0.75}]O_2$, where the most present honeycomb superstructure is lost on charging due to Mn migration that changes the coordination around O^{2-} and lowers the voltage on discharge.[120] As supported by DFT investigations, the ribbon superstructure in $Na_{0.6}[Li_{0.2}Mn_{0.8}]O_2$ inhibits manganese disorder and promotes stable electron holes on O^{2-}, hence suppressing O_2 formation and voltage hysteresis.[120] Ben Yahia *et al.* have used the electron localization function as a holistic tool to locate the oxygen lone pairs in the structure and follow their participation in the redox activity of layered oxides.[121] They propose the charge-transfer gap as the pertinent observable to quantify the amount of extra capacity achievable in charge and its reversibility in discharge. The idea of electron localization around oxygen ions is also present in the work by Zhao *et al.*, where it is shown to be favoured by Ti substitution leading to facilitated charge-transfer reaction for oxygen redox.[122] Clearly, the analysis of electronic structure can establish the energy levels positioning and allow the evaluation of several redox mechanisms. In early-TM-based oxides, O 2p states lie well below the TM d states, and the TMs mainly undertake the burden of the redox reaction. As going from early to late transition metals, the increased electronegativity enables larger overlapping between TM d and O p states, allowing the oxygen electron density to directly participate in the charge compensation.[123] In Li-rich oxides, *i.e.*, the alkali ion being present in both the alkali and TM layers, the O 2p orbitals overlap with the Li 2s orbitals and form Li^+–O–Li^+ interactions. The ionic nature of these interactions places the nonbonding O 2p states at the top of the valence band, which engage in anionic redox activity.[124] Maitra *et al.* reported that the presence of excess alkali metal is not necessary to trigger oxygen based processes, which can also take place in $Na_{2/3}[Mg_{0.28}Mn_{0.72}]O_2$ displaying Mg ions in the TM layer.[125] Charge compensation occurring along desodiation can be unveiled from electronic structure analysis performed as a function of Na content. Fig. 4 shows the trend of magnetization in each element sublattice for $Na_xNi_{0.25}Mn_{0.68}O_2$, where the Mn^{4+} oxidation state is essentially retained, while desodiation induces $Ni^{2+} \rightarrow Ni^{3+}$ and then $\rightarrow Ni^{4+}$ oxidation (Fig. 4a and b, respectively), in agreement with the literature.[126,127] The interested reader may be redirected to our previous work, where the oxidation trends are also confirmed by the TMO_6 octahedral distortion, with constant Mn–O pattern and shortening of Ni–O bonds along desodiation being associated to Jahn–Teller like effects.[128] The PDOS reported in Fig. 4c suggests a strong hybridization of TM d states with O p ones, leading to the highly covalent character of the TM–O bond, which would explain the resulting charge values far from the ionic limit (see Fig. 4d). However, a net variation of oxygen charge is still evident, and the formation of electron holes on oxygen atoms can also be evinced from the increased magnetization to $\sim$0.3 μ_B at xNa = 0.25 and up to $\sim$0.5 μ_B at xNa = 0.125. As also reported by Zhao *et al.* for the closely related $Na_{10-x}LiNi_3Mn_8O_{24}$ layered oxide, electron extraction would take

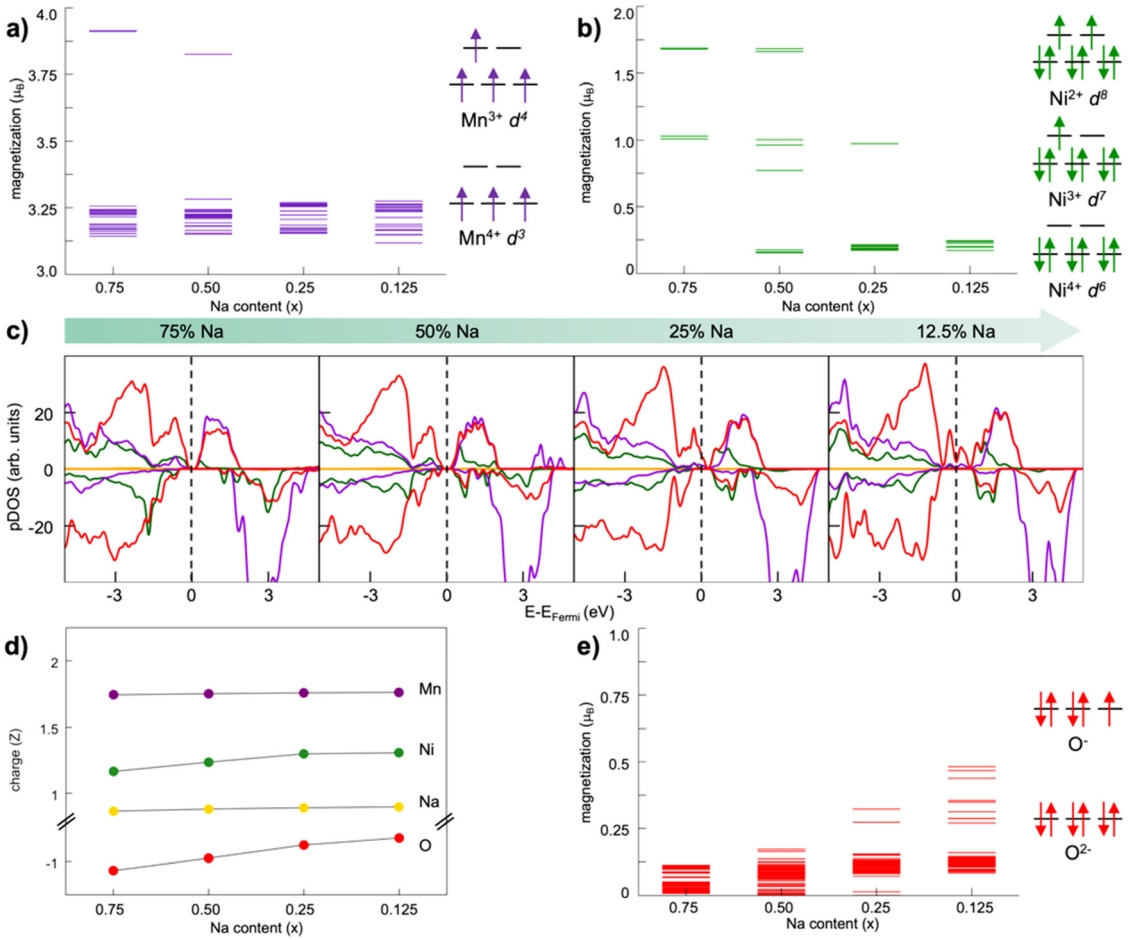

Fig. 4 Electronic structure analysis of $Na_xNi_{0.25}Mn_{0.68}O_2$ as a function of Na content: net magnetic moments on Mn (a) and Ni (b) species, with the corresponding electronic configuration on the side; (c) atom- and angular momentum-pDOS computed at the PBE+*U*(-D3BJ) level of theory; (d) Bader charge analysis reported as the average charge for each element; (e) net magnetic moment on O atoms with corresponding electronic configuration on the side. Colour code: Na s states, yellow; Mn d states, purple; Ni d states, green; O p states, red. Reproduced from ref. 128 [A. Massaro *et al.*, *ACS Energy Lett.*, 2021, **6**, 2470–2480]. Copyright 2021 American Chemical Society.[128]

place from Ni 3d states upon charge, and O 2p states start to participate at high desodiation degrees.[129]

3.2 The subtle balance between high voltage and reversible capacity: the importance of anionic redox chemistry

Oxygen redox activity can involve dimerization reactions, as experimentally observed but also computationally demonstrated.[123,130–132] Herein, the stabilization of oxygen dimers is key to endorse reversibility, and is shown to be managed *via* covalent TM substitutions.[123,130,131] For example, the surface lattice densification following oxygen release in $Na_{2/3}Ni_{1/3}Mn_{2/3}O_2$ and associated to large irreversible capacity loss was shown to be suppressed by Fe substitution.[133] The formation of dioxygen species at high voltage has been addressed in our group for the Mn-deficient phase of P2-type $Na_xNi_{0.25}Mn_{0.68}O_2$ layered oxides, where rational TM doping has been implemented at the Ni site.[128,134,135] The use of TM-defective oxides has attracted great consideration as a viable strategy to activate the anionic redox and thus enhance the specific capacity of layered oxides due to the emergence of nonbonding O 2p states.[136] However, the presence of a TM vacancy in the bulk lattice can represent a suitable site to accommodate the reactive oxygen species resulting from uncontrolled anionic redox. In principle, oxygen atoms can move from their regular positions in the crystalline lattice and form partially oxidized species (*i.e.*, peroxo-, superoxo-like) which can be accommodated near the Mn vacancy. The corresponding formation energy of the TM–O_2–TM intermediate, *i.e.*, the dioxygen binding to nearby TM atoms, can be computed as:

$$\Delta E = E_{\mathrm{TM\text{–}O_2\text{–}TM}} - E_{\mathrm{Na_xTMO_2}} \quad (6)$$

where $E_{\mathrm{TM\text{–}O_2\text{–}TM}}$ is the total energy of the dioxygen intermediate within the Na_xTMO_2 cathode lattice and $E_{\mathrm{Na_xTMO_2}}$ is the total energy of the material in its minimum-energy structure. As shown in Fig. 5, at low Na content the $Na_xNi_{0.25}Mn_{0.68}O_2$ cathode enables the formation of stable dioxygen species, that are mostly superoxides with $d_{O\text{–}O}$ ranging between 1.26 and 1.29 Å,[137,138] and binding the TM atoms in different modes (from bridging coordination to adjacent Ni and Mn atoms, to binuclear bridging to contiguous Mn atoms, or end-on to a single Mn atom), and even the complete release of molecular

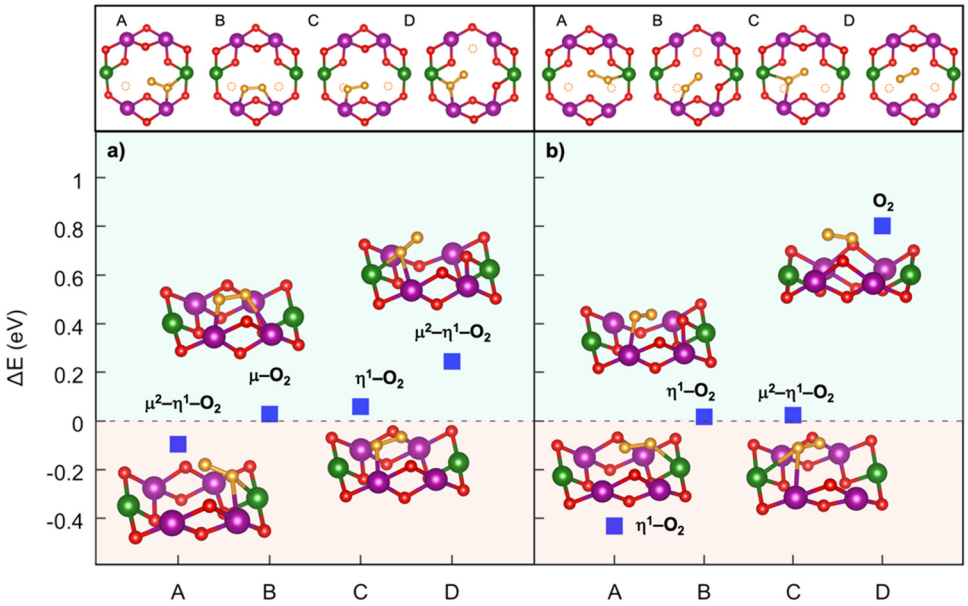

Fig. 5 Dioxygen formation in $Na_xNi_{0.25}Mn_{0.68}O_2$: (top) top-view of A–D structures and (bottom) dioxygen formation energetics identified at (a) *x*Na = 0.25 and (b) *x*Na = 0.125. Colour code: Ni, green; Mn, violet; O (lattice position), red; O (dioxygen position), orange; the yellow circles highlight the initial positions before dioxygen formation. Only atoms around the dioxygen complex are shown for clarity. Reproduced from ref. 128 [A. Massaro *et al.*, *ACS Energy Lett.*, 2021, **6**, 2470–2480]. Copyright 2021 American Chemical Society.[128]

oxygen with d_{O-O} of 1.23 Å and no direct coordination to any nearby TM atoms. The differences found in the energy values suggest that oxygen dimers are more easily formed when the oxygen atom leaves a Mn–O–Ni site rather than a Mn–O–Mn one. The energetically favourable dioxygen species at *x*Na = 0.25 (ΔE = −0.097 eV) explains the additional plateau beginning at 4.1 V observed during the first charge cycle, while the $\Delta E \sim 0.8$ eV associated to O_2 release is however easily accessible under NIB operating conditions and accounts for the irreversible capacity loss detected at 4.5 V.[126]

Implementing a stronger covalent nature for the TM–O bond *via* tailored substitution at the Ni site can represent an effective design strategy for reversible high-energy cathodes. Starting from promising evidence in the literature, Fe- and Ru-doping at the Ni site can be investigated.[133,139] On one hand, recent reports on Fe-doped Na_xTMO_2 cathodes show enhanced and reversible specific capacities that are imputable to oxygen redox with no detection of gaseous O_2.[133] On the other hand, the presence of Ru in Li-rich materials is known to accomplish the reversible access of oxygen redox: the electronic signatures of reversible O–O coupling in $Li_{2-x}RuO_3$ represent direct evidence of lattice oxygen redox activated at high voltage, and the oxygen dimerization mechanism in Ru-doped Li_2TMO_3 is shown to be hampered compared to other TM doping.[140–142] While Fe-containing oxides would also meet the low-cost and sustainability requirements,[110] it is crucial to balance the amount of Ru employed with the overall possible benefits. High cycle stability has also been reported for Na-rich Na_2RuO_3, where not only the honeycomb superstructure ordering, but also the presence of Ru plays a direct role in suppressing O_2 release.[143] From these considerations, dioxygen formation has also been addressed in $Na_xFe_{0.125}Ni_{0.125}Mn_{0.68}O_2$ and $Na_xRu_{0.125}Ni_{0.125}Mn_{0.68}O_2$ at low Na contents (see Fig. 6). The dimerization leads to superoxide species (d_{O-O} ∼1.26–1.37 Å for Fe-doped and 1.28–1.32 Å for Ru-doped) binding the TM atoms in bridging or binuclear bridging coordination modes. At *x*Na = 0.125, the $Na_xFe_{0.125}Ni_{0.125}Mn_{0.68}O_2$ cathode exhibits the most stable superoxide (ΔE = −0.197 eV) formed *via* breaking of the Ni–O bond. Panel b of Fig. 6 highlights the role of Ru in dioxygen formation, which can only be unfolded at *x*Na = 0.25 as lower Na compositions are tricky to model and predict.[139] Dimerization *via* Ru–O bond breaking is the most unlikely mechanism, leading to the highest-energy Mn–O_2–Ni configuration with ΔE = 3.283 eV and to the unfeasible Mn–O_2–Mn that actually restore back the strong Ru–O bond to form the same Mn–O_2–Ru structure with ΔE = 1.732 eV. Conversely to the undoped $Na_xNi_{0.25}Mn_{0.68}O_2$, the release of molecular O_2 is not predicted for the $Na_xFe_{0.125}Ni_{0.125}Mn_{0.68}O_2$ and $Na_xRu_{0.125}Ni_{0.125}Mn_{0.68}O_2$, thus proving the crucial role played by Fe and Ru in stabilizing the partially oxidized oxygen sublattice. The rather small amount of Fe/Ru doping seems to introduce the essential mild TM–O bond strengths that prevent the O_2 evolution while still enabling the activation of anionic redox processes *via* the formation of potentially reversible superoxide species. In this way, not only extra specific capacity can be achieved, but it can also be recovered upon subsequent charge/discharge cycles since O_2 release is suppressed or at least reduced.

The determination of dioxygen migration barriers may be relevant to obtain insightful predictions on the fate of oxygen evolution and assess the lattice role in activating and controlling the oxygen redox at the bulk state. However, multiple reaction pathways arising from such complex chemical frameworks

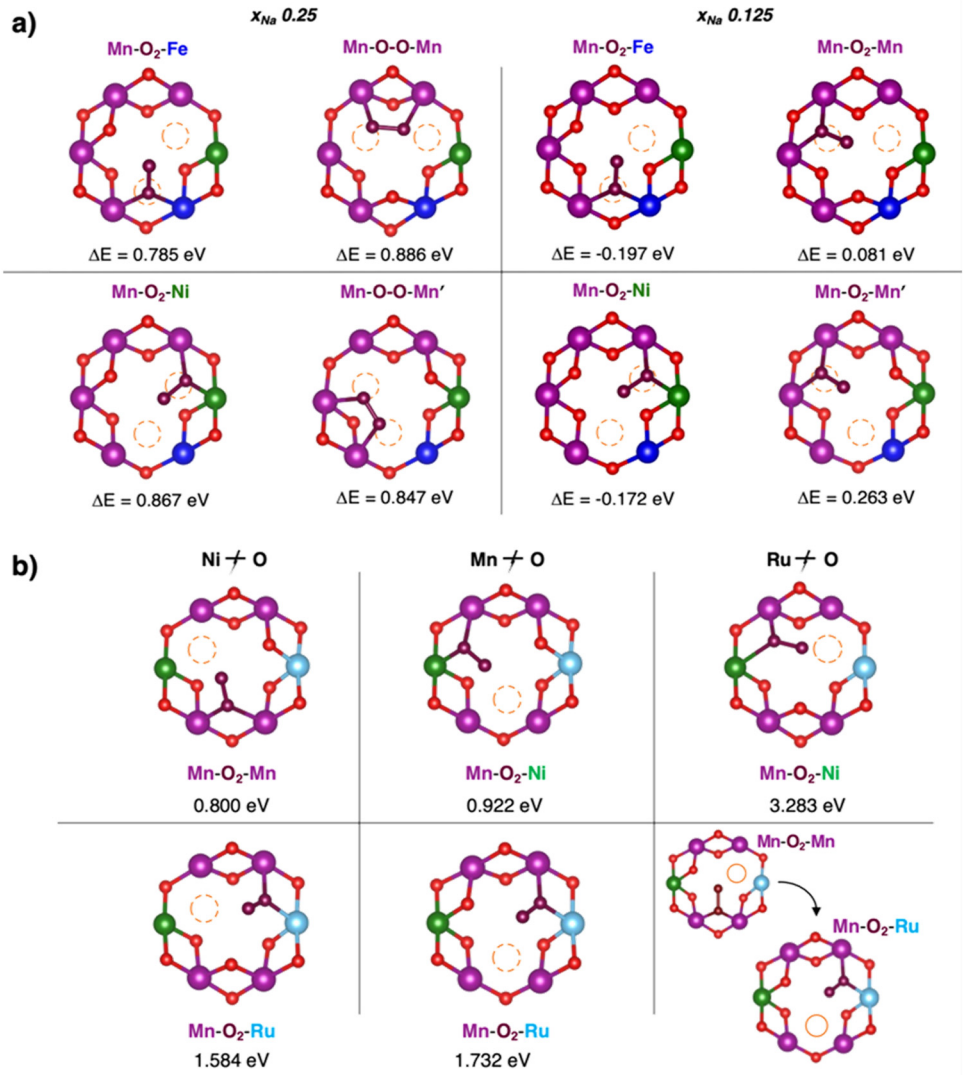

Fig. 6 Formation of dioxygen species in the Mn-deficient site of (a) $Na_{1/4}Fe_{1/8}Ni_{1/8}Mn_{3/4-y}O_2$ and (b) $Na_{1/4}Ru_{1/8}Ni_{1/8}Mn_{3/4-y}O_2$. Corresponding formation energy, ΔE, computed according to eqn (3) at PBE+U(-D3BJ) are also reported. Colour code as in Fig. 5, O atoms at dioxygen positions are depicted in brown, Fe in blue and Ru in cyan. Reproduced from ref. 134 [A. Massaro *et al.*, *J. Am. Ceram. Soc.*, 2023, **106**, 109–119]. Copyright ©2000–2022 by John Wiley & Sons, Inc.[134] Reproduced from ref. 135 [A. Massaro *et al.*, *ACS Appl. Energy Mater.*, 2022, **5**(9), 10721–10730]. Copyright 2022 American Chemical Society.[135]

(Na_xTMO_2, TM = Mn, Ni; Mn, Ni, Fe; Mn, Ni, Ru) lead to highly demanding calculations which will be addressed in the future. It is worth mentioning that comparison with more accurate hybrid-DFT methods would be recommended due to the poor GGA-PBE prediction on O_2 energy, and the interested reader is referred to the dedicated benchmark studies.[118,123,128]

3.3 Design principles towards highly effective cathodes: predicting oxygen evolution

The mechanism underlying dioxygen formation is sensitive to the chemical environment (*e.g.*, metal atoms that are involved upon breaking and formation of TM–O bonds). Indeed, very different outcomes are obtained with Ni-, Ni/Fe- and Ni/Ru-containing TM oxides. The intense debate in the literature on activation and control of oxygen-based redox in layered Na_xTMO_2 seems to agree in identifying the TM–O bond strength as a key factor which tuning strategies may be referred to. This property can be easily quantified in terms of oxygen vacancy formation energies: the lower the formation energy of a given V_O, the easier the tendency to break the involved chemical bonds. In a layered Na_xTMO_2, the reaction leading to the removal of one oxygen atom and thus to an O-defective material can be written as:

$$Na_xTMO_2 \rightarrow Na_xTMO_2^* + \frac{1}{2}O_2 \quad (7)$$

Therefore, the following equation should be considered to calculate the corresponding formation energy:

$$E_{V_O} = E_{def} - E_{prist} + \frac{1}{2}E_{O_2} \quad (8)$$

where E_{def} and E_{prist} are the total energies of, respectively, the oxygen vacancy (V_O) containing system and the pristine one, and E_{O_2} is the total energy of the oxygen molecule in its triplet ground state calculated at the same level of theory and used as a reference. This quantity can be considered as a direct measure of the TM–O bond strength: the lower the E_{V_O}, the easier the tendency to break the involved chemical bonds. While being widely applied to address open questions in materials science for several applications,[144,145] this idea is used here to show which TM doping would work more efficiently in reversible conditions. The thermodynamics of oxygen vacancy formation was first addressed in $Na_xNi_{0.25}Mn_{0.68}O_2$, where we have considered four types of vacancies differing for both the coordination to the Mn-deficient site (twofold or threefold coordinated, $V_O(2c)$ and $V_O(3c)$, respectively) and the chemical environment (consisting of only Mn sites or also Ni ones, V_O Mn/Mn and V_O Mn/Ni, respectively). Calculated values according to eqn (8) for each non-equivalent V_O at each Na content are listed in Table 2 and lie in the same energy range reported for a similar system, $Li_{1.2}Mn_{0.6}Ni_{0.2}O_2$.[146] The results show that: (i) oxygen vacancies are more likely to occur next to the Mn-deficient site rather than in the second coordination shell, as it is easier to remove a twofold coordinated oxygen atom than a threefold coordinated one ($E_{V_O}(2c) < E_{V_O}(3c)$); (ii) there is a general trend of decreasing formation energy with decreasing Na content due to charge compensation effects, leading to more favourable accommodation of reducing defects (V_O) in oxidized states (desodiated structures); (iii) Mn–V_O–Ni configurations are more convenient than Mn–V_O–Mn ones, as a result of the higher lability of the involved TM–O bonds (E_{V_O} Mn/Ni < E_{V_O} Mn/Mn).

Different kinds of twofold and threefold coordinated oxygen vacancies are then compared for the undoped material, $Na_xNi_{0.25}Mn_{0.68}O_2$, and the two doped ones, $Na_xFe_{0.125}Ni_{0.125}Mn_{0.68}O_2$ and $Na_xRu_{0.125}Ni_{0.125}Mn_{0.68}O_2$, at χ_{Na} = 0.25 (see Table 3). Formation energies for $V_O(2c)$ exhibit an altered trend: besides the Mn/Ni configuration showing the lowest E_{V_O} values in all materials, the effect of Ru doping is opposite compared to Fe, leading to E_{V_O} (Mn/Ru) > E_{V_O} (Mn). While Fe doping introduces mild TM–O covalency conditions, the presence of Ru atoms results in a significant strengthening of the chemical bond. The doping effects on the $V_O(3c)$ are more intertwined: removal of an oxygen atom is more difficult not only from Ru-, but also from Ni-containing configurations (E_{V_O} (Mn/Ru, Mn/Ni) > E_{V_O} (Mn)). On the other hand, Fe-doping always results in lowering the formation energies. In the most heterogenous site (*i.e.*, Mn/Ni/Ru), Ru and Ni seem to play a synergic effect that results in a higher E_{V_O} compared to E_{V_O} (Mn). Conversely, the E_{V_O} for Mn/Fe and Mn/Ni/Fe in $Na_xFe_{0.125}Ni_{0.125}Mn_{0.68}O_2$ are always lower than Mn and Mn/Ni ones, suggesting that the opposite effect of Ru doping compared to Fe is even exerted in the stabilization of the oxide moiety in a Ni-containing site.

Table 2 Oxygen vacancy formation energies computed at the PBE+*U*(-D3BJ) level of theory according to eqn (8). All the values are expressed in eV

*x*Na	$V_O(2c)$ Mn/Mn	$V_O(2c)$ Mn/Ni	$V_O(3c)$ Mn/Mn	$V_O(3c)$ Mn/Ni
0.75	1.866	2.623	3.204	3.443
0.50	1.944	1.447	2.865	2.858
0.25	1.515	1.079	2.454	2.587
0.125	1.077	0.114	2.537	2.390

Table 3 Comparison of oxygen vacancy formation energies in the three case-study materials (NNMO, $Na_xNi_{0.25}Mn_{0.68}O_2$; NFNMO, $Na_xFe_{0.125}Ni_{0.125}Mn_{0.68}O_2$; NRNMO $Na_xRu_{0.125}Ni_{0.125}Mn_{0.68}O_2$) at χ_{Na} = 0.25 computed at the PBE+*U*(-D3BJ) level of theory according to eqn (8). All the energy values are expressed in eV

$V_O(2c)$	Mn	Mn/Ni	Mn/Fe	Mn/Ru
NNMO	1.515	1.079	—	—
NFNMO	1.587	1.152	1.397	—
NRNMO	1.404	1.101	—	2.498

$V_O(3c)$	Mn	Mn/Ni	Mn/Fe	Mn/Ru	Mn/Ni/Fe	Mn/Ni/Ru
NNMO	2.454	2.587	—	—	—	—
NFNMO	2.635	2.335	1.899	—	1.634	—
NRNMO	2.435	3.328	—	3.121	—	2.983

We should recall that similar dopants (*i.e.*, Mn, Ni, Fe, and Ru) have been extensively investigated in LIB counterparts and are currently sought after for next-generation K-ion batteries (KIBs).[147–149] A superior performance has been reported for Mn- and Fe-rich layered oxides, which would also meet the sustainability requirements necessary for post-lithium technologies. Nickel incorporation is always beneficial to the overall energy density, thanks to the decreased Jahn-Teller distortion within the dominant Mn sublattice, while the presence of Ru has also been associated to improved structural support.[147–149] Research on layered oxides has taken great advantage from earlier efforts and discoveries as LIB cathodes, granting the rational development of novel positive electrodes on a fast-track. Fundamental understanding of structural retention, phase evolution, charge compensation mechanisms, reversible capacity, and high-voltage behaviour in these materials has endorsed significant remarks that are widely applicable to either Na- or K-based counterparts.

These new insights into anionic redox activity highlight simple descriptors able to predict the oxygen evolution from a certain structure and the critical state of charge for irreversible material degradation. The charge compensation mechanism driven by partially oxidized oxygen atoms and suggested by experiments is unfolded by means of readily computable quantities, such as oxygen vacancy formation and TM–O_2 coordination energy. These findings can be used to prevent O_2 release and improve the efficiency of high-energy cathodes able to recover the extra specific capacity upon subsequent cycling.

The broad theoretical literature on layered oxides is closely intertwined with experimental investigations. On one hand, the in-depth understanding of structural evolution and anionic redox is effectively enabled by atomistic simulations and electronic structure methods. On the other hand, direct connection to experimental data is required to ascertain a reliable description of complex and intricate chemical features evolving upon

the electrochemical sodiation/desodiation. After appropriate validation with experiments, our theoretical remarks on $Na_xNi_{0.25}Mn_{0.68}O_2$, $Na_xFe_{0.125}Ni_{0.125}Mn_{0.68}O_2$, and $Na_xRu_{0.125}Ni_{0.125}Mn_{0.68}O_2$ shed light on charge compensation mechanisms upon desodiation and anionic redox processes that are directly related to the electrochemical behaviour detected in the experiments, thus enriching the theoretical investigation with great predictive power.[126,127,129,133,139] As proved by the publications trend in the field, this kind of analysis has empowered the rational design of specific TM compositions, the introduction of functional point defects (*e.g.*, metal vacancy, TM doping), or voltage-controlled cycling.[150–154]

4. Conclusions and perspectives

This perspective article aims at providing an overview on the crucial role of computational chemistry and QM-based simulations in describing nanostructured electrode materials that are relevant for Na-ion battery applications. By accessing electronic structure and sodiation/desodiation mechanistic details at the nanoscale, QM-based methods enable the fundamental understanding of redox reactions, ion diffusion, and the role of defects along the charging/discharging process. Whether setting foundations for advancing multiscale techniques or delivering fundamental knowledge on electroactive materials, DFT simulations represent a powerful predictive tool towards new rational design strategies and offer an atomistic outlook for investigating reaction kinetics, electrochemical potentials, chemical stability, defects chemistry, and adsorption/dissociation energetics.

We have briefly illustrated how the recent literature in the field of Na-ion batteries has been enriched with design principles derived from first-principles theoretical investigations. State-of-the-art computational tools are shown to unveil new details on relevant topics, highlighting key features in nanostructured electrode materials that directly affect the sodiation/desodiation mechanisms.

Na^+ adsorption, intercalation and migration mechanisms are dissected for several nanostructured anodes: surface morphology and sodium radius, binding strength and steric hinderance are all intertwined features to take appropriately into account in order to obtain a conclusive picture of NIB electrode functioning mechanisms. The inclusion of a sawtooth-like potential has been proven to be a useful tool to efficiently describe how the electric field can control the Na^+ electrode interactions and paves the route towards realistic simulations of *in operando* conditions.

Charge compensation in high-energy layered oxides can be unfolded to outline tuneable activation of reversible anionic-redox active cathodes. More labile TM–O bonds undergo preferential cleavage towards superoxide formation and can be responsible for the full release of molecular oxygen, which can be suppressed by increasing the TM–O covalency.

Overall, our results contribute to shed light on the electrochemical behaviour of promising NIB systems and can drive future strategies for an effective tuning of heterogeneous functional materials. While explaining experimental observations and showing to what extent the key Na migration, charge compensation, anionic redox chemistry, etc., are reliably addressed by first-principles calculations, these findings and the identification of readily computable structural descriptors can be instrumental for the rational design and fast development of novel electrodes. Moreover, the described methodology can be extended to similar systems and set solid foundations for multiscale frameworks able to integrate systems and processes across several scales of space and time.

Over the last two decades, the accuracy and robustness of *ab initio* methods have enabled the in-depth understanding of complex electrochemical behaviors at the atomistic level. The huge impact of computer power in chemistry and energy related fields has been rapidly growing, up to the point that many technical challenges are overcome, and even automated simulations can be supplied with the advent of data mining and machine learning techniques. Notwithstanding these advances, every DFT calculation requires input structure models, and any computation becomes meaningless with no conception of the relevant material phases or invalid assumptions about the atomic structure. Although thermodynamically stable phases can be generally discovered, it is still challenging to predict metastable phases that may be present under operating conditions, such as nanostructures, polymorphs, or disordered phases. The eventual lack of information on the material structural evolution prevents the possibility of making quantitative predictions, thus hampering the computational design of entirely new materials. So far, most of the first-principles methods in battery research have been focused on crystalline solids, but the need for reliable models of non-crystalline solid-electrolyte interfaces is rapidly emerging as a key aspect to unveil many other battery features. The simulation of such complex structures typically requires large length scales that may be accessible by means of non-conventional multiscale methodologies beyond first principles. Still, major efforts should drive the full comprehension of complex phenomena occurring at heterogeneous electrochemical interfaces. Tricky reactivity, charge and mass transport processes may span different time scales and involve species with intrinsically different chemical natures (*i.e.*, metals, radicals). Great steps forward in *ab initio* modelling should definitely deal with these new challenges and the upcoming demand of gaining an integrated, unique theoretical perspective on – as real as possible – material models.

A fundamental understanding of battery functioning mechanisms will strongly benefit from upscaled-computational analysis, in view of the close cooperation between theory and experiments as unavoidable driving forces to foster innovation and production of much needed highly performing NIB devices.

Conflicts of interest

The authors declare no conflicts of interests.

Acknowledgements

The authors acknowledge European Union (FSE, PON Ricerca e Innovazione 2014–2020, Azione I.1 ''Dottorati Innovativi con caratterizzazione Industriale''), for funding a PhD grant to Arianna Massaro. Part of this work was carried out within the activities ''Ricerca Sistema Elettrico'' funded through contributions to research and development by the Italian Ministry of Economic Development. The computing resources and the related technical support used for this work have been provided by CRESCO/ENEAGRID High Performance Computing infrastructure and its staff;[155] CRESCO/ENEAGRID High Performance Computing infrastructure is funded by ENEA, the Italian National Agency for New Technologies, Energy and Sustainable Economic Development and by Italian and European research programs, see: **http://www.cresco.enea.it/english** for further information.

References

1 J. B. Goodenough and K.-S. Park, The Li-Ion Rechargeable Battery: A Perspective, *J. Am. Chem. Soc.*, 2013, **135**, 1167–1176.
2 J. B. Goodenough and Y. Kim, Challenges for Rechargeable Li Batteries, *Chem. Mater.*, 2010, **22**, 587–603.
3 B. Nykvist and M. Nilsson, Rapidly Falling Costs of Battery Packs for Electric Vehicles, *Nat. Clim. Change*, 2015, **5**, 329–332.
4 D. Larcher and J. M. Tarascon, Towards greener and more sustainable batteries for electrical energy storage, *Nat. Chem.*, 2015, **7**, 19–29.
5 G. E. Blomgren, The Development and Future of Lithium Ion Batteries, *J. Electrochem. Soc.*, 2017, **164**, A5019–A5025.
6 K. M. Abraham, How Comparable Are Sodium-Ion Batteries to Lithium-Ion Counterparts?, *ACS Energy Lett.*, 2020, **5**, 3544–3547.
7 P. K. Nayak, L. Yang, W. Brehm and P. Adelhelm, From Lithium-Ion to Sodium-Ion Batteries: Advantages, Challenges, and Surprises, *Angew. Chem., Int. Ed.*, 2018, **57**, 102–120.
8 K. Chayambuka, G. Mulder, D. L. Danilov and P. H. L. Notten, Sodium-Ion Battery Materials and Electrochemical Properties Reviewed, *Adv. Energy Mater.*, 2018, **8**, 1800079.
9 Y. Huang, Y. Zheng, X. Li, F. Adams, W. Luo, Y. Huang and L. Hu, Electrode Materials of Sodium-Ion Batteries toward Practical Application, *ACS Energy Lett.*, 2018, **3**, 1604–1612.
10 J. Y. Hwang, S. T. Myung and Y. K. Sun, Sodium-ion batteries: Present and future, *Chem. Soc. Rev.*, 2017, **46**, 3529–3614.
11 Y. Fang, X.-Y. Yu and X. W. Lou, Nanostructured Electrode Materials for Advanced Sodium-Ion Batteries, *Matter*, 2019, **1**, 90–114.
12 P. G. Bruce, B. Scrosati and J. M. Tarascon, Nanomaterials for rechargeable lithium batteries, *Angew. Chem., Int. Ed.*, 2008, **47**, 2930–2946.
13 M. C. Masedi, P. E. Ngoepe and H. M. Sithole, Beyond lithium-ion batteries: A computational study on Na-S and Na-O batteries, *IOP Conf. Ser. Mater. Sci. Eng.*, 2017, **169**, 012001.
14 R. Jayan and M. M. Islam, Mechanistic Insights into Interactions of Polysulfides at VS_2 Interfaces in Na–S Batteries: A DFT Study, *ACS Appl. Mater. Interfaces*, 2021, **13**, 35848–35855.
15 T. Kaewmaraya, T. Hussain, R. Umer, Z. Hu and X. S. Zhao, Efficient suppression of the shuttle effect in Na–S batteries with an As_2 S_3 anchoring monolayer, *Phys. Chem. Chem. Phys.*, 2020, **22**, 27300–27307.
16 R. Jayan and M. M. Islam, Single-Atom Catalysts for Improved Cathode Performance in Na–S Batteries: A Density Functional Theory (DFT) Study, *J. Phys. Chem. C*, 2021, **125**, 4458–4467.
17 Z. Zheng, J. Jiang, H. Guo, C. Li, K. Konstantinov, Q. Gu and J. Wang, Tuning NaO_2 formation and decomposition routes with nitrogen-doped nanofibers for low overpotential Na-O_2 batteries, *Nano Energy*, 2021, **81**, 105529.
18 L. M. Morgan, M. P. Mercer, A. Bhandari, C. Peng, M. M. Islam, H. Yang, J. Holland, S. W. Coles, R. Sharpe, A. Walsh, B. J. Morgan, D. Kramer, M. S. Islam, H. E. Hoster, J. S. Edge and C.-K. Skylaris, Pushing the boundaries of lithium battery research with atomistic modelling on different scales, *Prog. Energy*, 2022, **4**, 012002.
19 H. Euchner and A. Groß, Atomistic modeling of Li- and post-Li-ion batteries, *Phys. Rev. Mater.*, 2022, **6**, 040302.
20 J. Lee, A. Urban, X. Li, D. Su, G. Hautier and G. Ceder, Unlocking the Potential of Cation-Disordered Oxides for Rechargeable Lithium Batteries, *Science*, 2014, **343**, 519–522.
21 G. Åvall, J. Mindemark, D. Brandell and P. Johansson, Sodium-Ion Battery Electrolytes: Modeling and Simulations, *Adv. Energy Mater.*, 2018, **8**, 1703036.
22 Z.-T. Sun and S.-H. Bo, Understanding electro-mechanical-thermal coupling in solid-state lithium metal batteries *via* phase-field modeling, *J. Mater. Res.*, 2022, **37**, 3130–3145.
23 T. Shi, Q. Tu, Y. Tian, Y. Xiao, L. J. Miara, O. Kononova and G. Ceder, High Active Material Loading in All-Solid-State Battery Electrode *via* Particle Size Optimization, *Adv. Energy Mater.*, 2020, **10**, 1902881.
24 J. M. Reniers, G. Mulder and D. A. Howey, Review and Performance Comparison of Mechanical-Chemical Degradation Models for Lithium-Ion Batteries, *J. Electrochem. Soc.*, 2019, **166**, A3189–A3200.
25 C. D. Parke, L. Teo, D. T. Schwartz and V. R. Subramanian, Progress on continuum modeling of lithium–sulfur batteries, *Sustainable Energy Fuels*, 2021, **5**, 5946–5966.
26 J. Popovic, D. Brandell, S. Ohno, K. B. Hatzell, J. Zheng and Y.-Y. Hu, Polymer-based hybrid battery electrolytes: theoretical insights, recent advances and challenges, *J. Mater. Chem. A*, 2021, **9**, 6050–6069.
27 R. P. Carvalho, C. F. N. Marchiori, C. M. Araujo and D. Brandell, *Redox Polymers for Energy and Nanomedicine*, The Royal Society of Chemistry, 2020, pp. 93–136.
28 O. Borodin, G. D. Smith, R. Bandyopadhyaya and O. Byutner, Molecular Dynamics Study of the Influence

of Solid Interfaces on Poly(ethylene oxide) Structure and Dynamics, *Macromolecules*, 2003, **36**, 7873–7883.
29 O. Borodin and G. D. Smith, Development of Many−Body Polarizable Force Fields for Li-Battery Applications: 2. LiTFSI-Doped Oligoether, Polyether, and Carbonate-Based Electrolytes, *J. Phys. Chem. B*, 2006, **110**, 6293–6299.
30 O. N. Starovoytov, Development of a Polarizable Force Field for Molecular Dynamics Simulations of Lithium-Ion Battery Electrolytes: Sulfone-Based Solvents and Lithium Salts, *J. Phys. Chem. B*, 2021, **125**, 11242–11255.
31 A. Massaro, J. Avila, K. Goloviznina, I. Rivalta, C. Gerbaldi, M. Pavone, M. F. Costa Gomes and A. A. H. Padua, Sodium diffusion in ionic liquid-based electrolytes for Na-ion batteries: the effect of polarizable force fields, *Phys. Chem. Chem. Phys.*, 2020, **22**, 20114–20122.
32 Z. Shi, J. Zhou and R. Li, Application of Reaction Force Field Molecular Dynamics in Lithium Batteries, *Front. Chem.*, 2021, **8**, 634379.
33 T. C. Lourenço, M. Ebadi, D. Brandell, J. L. F. Da Silva and L. T. Costa, Interfacial Structures in Ionic Liquid-Based Ternary Electrolytes for Lithium-Metal Batteries: A Molecular Dynamics Study, *J. Phys. Chem. B*, 2020, **124**, 9648–9657.
34 L. Zhang, J. Han, H. Wang, R. Car and E. Weinan, Deep Potential Molecular Dynamics: A Scalable Model with the Accuracy of Quantum Mechanics, *Phys. Rev. Lett.*, 2018, **120**, 143001.
35 J. Behler and M. Parrinello, Generalized Neural-Network Representation of High-Dimensional Potential-Energy Surfaces, *Phys. Rev. Lett.*, 2007, **98**, 146401.
36 H. Guo, Q. Wang, A. Stuke, A. Urban and N. Artrith, Accelerated Atomistic Modeling of Solid-State Battery Materials With Machine Learning, *Front. Energy Res.*, 2021, **9**, 695902.
37 V. L. Deringer, Modelling and understanding battery materials with machine-learning-driven atomistic simulations, *J. Phys. Energy*, 2020, **2**, 041003.
38 Q. He, B. Yu, Z. Li and Y. Zhao, Density Functional Theory for Battery Materials, *Energy Environ. Mater.*, 2019, **2**, 264–279.
39 X. Li, X. Chen, Q. Bai, Y. Mo and Y. Zhu, From atomistic modeling to materials design: computation-driven material development in lithium-ion batteries, *Sci. China: Chem.*, 2023, 1–15.
40 D. A. Aksyonov, A. O. Boev, S. S. Fedotov and A. M. Abakumov, Computational insights into ionic conductivity of transition metal electrode materials for metal-ion batteries - A review, *Solid State Ionics*, 2023, **393**, 116170.
41 S. Zhang, J. Ma, S. Dong and G. Cui, Designing All-Solid-State Batteries by Theoretical Computation: A Review, *Electrochem. Energy Rev.*, 2023, **6**, 4.
42 V. I. Anisimov, J. Zaanen and O. K. Andersen, Band theory and Mott insulators: Hubbard U instead of Stoner I, *Phys. Rev. B: Condens. Matter Mater. Phys.*, 1991, **44**, 943–954.
43 S. A. Tolba, K. M. Gameel, B. A. Ali, H. A. Almossalami and N. K. Allam, *Density Functional Calculations - Recent Progresses of Theory and Application*, InTech, 2018, pp. 3–30.
44 S. Lutfalla, V. Shapovalov and A. T. Bell, Calibration of the DFT/GGA+*U* Method for Determination of Reduction Energies for Transition and Rare Earth Metal Oxides of Ti, V, Mo, and Ce, *J. Chem. Theory Comput.*, 2011, **7**, 2218–2223.
45 L. Wang, T. Maxisch and G. Ceder, Oxidation energies of transition metal oxides within the GGA+*U* framework, *Phys. Rev. B: Condens. Matter Mater. Phys.*, 2006, **73**, 195107.
46 S. Grimme, J. Antony, S. Ehrlich and H. Krieg, A consistent and accurate ab initio parametrization of density functional dispersion correction (DFT-D) for the 94 elements H-Pu, *J. Chem. Phys.*, 2010, **132**, 154104.
47 V. Barone, M. Casarin, D. Forrer, M. Pavone, M. Sambi and A. Vittadini, Role and effective treatment of dispersive forces in materials: Polyethylene and graphite crystals as test cases, *J. Comput. Chem.*, 2009, **30**, 934–939.
48 A. Pecoraro, E. Schiavo, P. Maddalena, A. B. Muñoz-García and M. Pavone, Structural and electronic properties of defective 2D transition metal dichalcogenide heterostructures, *J. Comput. Chem.*, 2020, **41**, 1946–1955.
49 A. B. Muñoz-García, A. Massaro and M. Pavone, Ab initio study of $PbCr_{(1-x)}S_xO4$ solid solution: an inside look at Van Gogh Yellow degradation, *Chem. Sci.*, 2016, **7**, 4197–4203.
50 P. E. Blöchl, Projector augmented-wave method, *Phys. Rev. B: Condens. Matter Mater. Phys.*, 1994, **50**, 17953–17979.
51 G. Kresse and J. Furthmüller, Efficient iterative schemes for ab initio total-energy calculations using a plane-wave basis set, *Phys. Rev. B: Condens. Matter Mater. Phys.*, 1996, **54**, 11169–11186.
52 J. Neugebauer and M. Scheffler, Adsorbate-substrate and adsorbate-adsorbate interactions of Na and K adlayers on Al(111), *Phys. Rev. B: Condens. Matter Mater. Phys.*, 1992, **46**, 16067–16080.
53 V. L. Chevrier and G. Ceder, Challenges for Na-ion Negative Electrodes, *J. Electrochem. Soc.*, 2011, **158**, A1011.
54 G. Longoni, R. L. Pena Cabrera, S. Polizzi, M. D'Arienzo, C. M. Mari, Y. Cui and R. Ruffo, Shape-Controlled TiO_2 Nanocrystals for Na-Ion Battery Electrodes: The Role of Different Exposed Crystal Facets on the Electrochemical Properties, *Nano Lett.*, 2017, **17**, 992–1000.
55 L. David, R. Bhandavat and G. Singh, MoS_2/graphene composite paper for sodium-ion battery electrodes, *ACS Nano*, 2014, **8**, 1759–1770.
56 W. Lu, Z. Wang and S. Zhong, Sodium-ion battery technology: Advanced anodes, cathodes and electrolytes, *J. Phys. Conf. Ser.*, 2021, **2109**, 012004.
57 F. Fasulo, A. B. Muñoz-García, A. Massaro, O. Crescenzi, C. Huang and M. Pavone, Vinylene carbonate reactivity at lithium metal surface: first-principles insights into the early steps of SEI formation, *J. Mater. Chem. A*, 2023, **11**, 5660–5669.
58 E. Peled and S. Menkin, Review—SEI: Past, Present and Future, *J. Electrochem. Soc.*, 2017, **164**, A1703–A1719.
59 Y. Cao, L. Xiao, M. L. Sushko, W. Wang, B. Schwenzer, J. Xiao, Z. Nie, L. V. Saraf, Z. Yang and J. Liu, Sodium Ion Insertion in Hollow Carbon Nanowires for Battery Applications, *Nano Lett.*, 2012, **12**, 3783–3787.
60 P.-C. Tsai, S.-C. Chung, S.-K. Lin and A. Yamada, Ab initio study of sodium intercalation into disordered carbon, *J. Mater. Chem. A*, 2015, **3**, 9763–9768.

61 C.-Y. Chou, M. Lee and G. S. Hwang, A Comparative First-Principles Study on Sodiation of Silicon, Germanium, and Tin for Sodium-Ion Batteries, *J. Phys. Chem. C*, 2015, **119**, 14843–14850.
62 M. Mayo, K. J. Griffith, C. J. Pickard and A. J. Morris, Ab Initio Study of Phosphorus Anodes for Lithium- and Sodium-Ion Batteries, *Chem. Mater.*, 2016, **28**, 2011–2021.
63 Q. Bai, L. Yang, H. Chen and Y. Mo, Computational Studies of Electrode Materials in Sodium-Ion Batteries, *Adv. Energy Mater.*, 2018, **8**, 1702998.
64 G. Henkelman, B. P. Uberuaga and H. Jónsson, A climbing image nudged elastic band method for finding saddle points and minimum energy paths, *J. Chem. Phys.*, 2000, **113**, 9901–9904.
65 E. Irisarri, A. Ponrouch and M. R. Palacin, Review—Hard Carbon Negative Electrode Materials for Sodium-Ion Batteries, *J. Electrochem. Soc.*, 2015, **162**, A2476–A2482.
66 M. N. Obrovac and V. L. Chevrier, Alloy Negative Electrodes for Li-Ion Batteries, *Chem. Rev.*, 2014, **114**, 11444–11502.
67 U. Arrieta, N. A. Katcho, O. Arcelus and J. Carrasco, First-principles study of sodium intercalation in crystalline Na_xSi_{24} ($0 \leq x \leq 4$) as anode material for na-ion batteries, *Sci. Rep.*, 2017, **7**, 1–8.
68 V. Sharma, K. Ghatak and D. Datta, Amorphous germanium as a promising anode material for sodium ion batteries: a first principle study, *J. Mater. Sci.*, 2018, **53**, 14423–14434.
69 A. Majid, K. Hussain, S. Ud-Din Khan and S. Ud-Din Khan, First principles study of SiC as the anode in sodium ion batteries, *New J. Chem.*, 2020, **44**, 8910–8921.
70 S. Dhillon, G. Hernández, N. P. Wagner, A. M. Svensson and D. Brandell, Modelling capacity fade in silicon–graphite composite electrodes for lithium-ion batteries, *Electrochim. Acta*, 2021, **377**, 138067.
71 R. P. Carvalho, C. F. N. Marchiori, V.-A. Oltean, S. Renault, T. Willhammar, C. Pay Gómez, C. M. Araujo and D. Brandell, Structure–property relationships in organic battery anode materials: exploring redox reactions in crystalline Na- and Li-benzene diacrylate using combined crystallography and density functional theory calculations, *Mater. Adv.*, 2021, **2**, 1024–1034.
72 Y. Lu, Y. Lu, Z. Niu and J. Chen, Graphene-Based Nanomaterials for Sodium-Ion Batteries, *Adv. Energy Mater.*, 2018, **8**, 1–21.
73 J. Shuai, H. D. Yoo, Y. Liang, Y. Li, Y. Yao and L. C. Grabow, Density functional theory study of Li, Na, and Mg intercalation and diffusion in MoS_2 with controlled interlayer spacing, *Mater. Res. Express*, 2016, **3**, 1–8.
74 X. Xie, Z. Ao, D. Su, J. Zhang and G. Wang, MoS_2/Graphene Composite Anodes with Enhanced Performance for Sodium-Ion Batteries: The Role of the Two-Dimensional Heterointerface, *Adv. Funct. Mater.*, 2015, **25**, 1393–1403.
75 L. Wang, H. Zhang, Y. Wang, C. Qian, Q. Dong, C. Deng, D. Jiang, M. Shu, S. Pan and S. Zhang, Unleashing ultra-fast sodium ion storage mechanisms in interface-engineered monolayer MoS_2/C interoverlapped superstructure with robust charge transfer networks, *J. Mater. Chem. A*, 2020, **8**, 15002–15011.
76 A. Massaro, A. Pecoraro, A. Muñoz-García and M. Pavone, First-Principles Study of Na Intercalation and Diffusion Mechanisms at 2D MoS_2/Graphene Interfaces, *J. Phys. Chem. C*, 2021, **125**, 2276–2286.
77 D. Sun, D. Huang, H. Wang, G.-L. Xu, X. Zhang, R. Zhang, Y. Tang, D. Abd EI-Hady, W. Alshitari, A. Saad AL-Bogami, K. Amine and M. Shao, 1T MoS_2 nanosheets with extraordinary sodium storage properties *via* thermal-driven ion intercalation assisted exfoliation of bulky MoS_2, *Nano Energy*, 2019, **61**, 361–369.
78 J. Su, Y. Pei, Z. Yang and X. Wang, Ab initio study of graphene-like monolayer molybdenum disulfide as a promising anode material for rechargeable sodium ion batteries, *RSC Adv.*, 2014, **4**, 43183–43188.
79 G. Barik and S. Pal, Defect Induced Performance Enhancement of Monolayer MoS_2 for Li- and Na-Ion Batteries, *J. Phys. Chem. C*, 2019, **123**, 21852–21865.
80 E. Olsson, G. Chai, M. Dove and Q. Cai, Adsorption and migration of alkali metals (Li, Na, and K) on pristine and defective graphene surfaces, *Nanoscale*, 2019, **11**, 5274–5284.
81 J. Shuai, H. D. Yoo, Y. Liang, Y. Li, Y. Yao and L. C. Grabow, Density functional theory study of Li, Na, and Mg intercalation and diffusion in MoS_2 with controlled interlayer spacing, *Mater. Res. Express*, 2016, **3**, 064001.
82 D. Sun, D. Ye, P. Liu, Y. Tang, J. Guo, L. Wang and H. Wang, MoS_2/Graphene Nanosheets from Commercial Bulky MoS_2 and Graphite as Anode Materials for High Rate Sodium-Ion Batteries, *Adv. Energy Mater.*, 2018, **8**, 1702383.
83 M. K. Singh, J. Pati, D. Seth, J. Prasad, M. Agarwal, M. A. Haider, J.-K. Chang and R. S. Dhaka, Diffusion mechanism and electrochemical investigation of 1T phase Al–MoS_2@rGO nano-composite as a high-performance anode for sodium-ion batteries, *Chem. Eng. J.*, 2023, **454**, 140140.
84 J. Xiao, J. Zhou, L.-N. Chen and J. Chen, Na transport in bilayer MoS_2 and MoS_2-WS_2 heterojunction with S vacancy defect: First-principles study, *AIP Adv.*, 2022, **12**, 65218.
85 J. Wang, X. Zheng, Y. Dong, L. Chen, L. Chen and W. He, Reactant conversion–intercalation strategy toward interlayer-expanded MoS_2 microflowers with superior supercapacitor performance, *Dalton Trans.*, 2023, **52**, 4537–4547.
86 K. Chiba, N. Kijima, Y. Takahashi, Y. Idemoto and J. Akimoto, Synthesis, structure, and electrochemical Li-ion intercalation properties of $Li_2Ti_3O_7$ with $Na_2Ti_3O_7$-type layered structure, *Solid State Ionics*, 2008, **178**, 1725–1730.
87 G. Rousse, M. E. Arroyo-de Dompablo, P. Senguttuvan, A. Ponrouch, J.-M. Tarascon and M. R. Palacín, Rationalization of Intercalation Potential and Redox Mechanism for $A_2Ti_3O_7$ (A = Li, Na), *Chem. Mater.*, 2013, **25**, 4946–4956.
88 J. Xu, C. Ma, M. Balasubramanian and Y. S. Meng, Understanding $Na_2Ti_3O_7$ as an ultra-low voltage anode material for a Na-ion battery, *Chem. Commun.*, 2014, **50**, 12564–12567.

89 L. Wu, D. Bresser, D. Buchholz, G. A. Giffin, C. R. Castro, A. Ochel and S. Passerini, Unfolding the Mechanism of Sodium Insertion in Anatase TiO_2 Nanoparticles, *Adv. Energy Mater.*, 2015, **5**, 1401142.
90 X. Yang, C. Wang, Y. Yang, Y. Zhang, X. Jia, J. Chen and X. Ji, Anatase TiO_2 nanocubes for fast and durable sodium ion battery anodes, *J. Mater. Chem. A*, 2015, **3**, 8800–8807.
91 A. Massaro, A. B. Muñoz-García, P. Maddalena, F. Bella, G. Meligrana, C. Gerbaldi and M. Pavone, First-principles study of Na insertion at TiO_2 anatase surfaces: new hints for Na-ion battery design, *Nanoscale Adv.*, 2020, **2**, 2745–2751.
92 F. Bella, A. B. Muñoz-García, G. Meligrana, A. Lamberti, M. Destro, M. Pavone and C. Gerbaldi, Unveiling the controversial mechanism of reversible Na storage in TiO_2 nanotube arrays: Amorphous versus anatase TiO_2, *Nano Res.*, 2017, **10**, 2891–2903.
93 Z. Bayhan, G. Huang, J. Yin, X. Xu, Y. Lei, Z. Liu and H. N. Alshareef, Two-Dimensional TiO 2 /TiS 2 Hybrid Nanosheet Anodes for High-Rate Sodium-Ion Batteries, *ACS Appl. Energy Mater.*, 2021, **4**, 8721–8727.
94 K. Leung, L. C. Merrill and K. L. Harrison, Galvanic Corrosion and Electric Field in Lithium Anode Passivation Films: Effects on Self-Discharge, *J. Phys. Chem. C*, 2022, **126**, 8565–8580.
95 K. Leung, DFT modelling of explicit solid–solid interfaces in batteries: methods and challenges, *Phys. Chem. Chem. Phys.*, 2020, **22**, 10412–10425.
96 F. Fasulo, A. Massaro, A. B. Muñoz-García and M. Pavone, Na uptake at TiO_2 anatase surfaces under electric field control: A first-principles study, *J. Mater. Res.*, 2022, **37**, 3216–3226.
97 S. Selçuk and A. Selloni, Influence of external electric fields on oxygen vacancies at the anatase (101) surface, *J. Chem. Phys.*, 2014, **141**, 084705.
98 D. Atkins, E. Ayerbe, A. Benayad, F. G. Capone, E. Capria, I. E. Castelli, I. Cekic-Laskovic, R. Ciria, L. Dudy, K. Edström, M. R. Johnson, H. Li, J. M. G. Lastra, M. L. De Souza, V. Meunier, M. Morcrette, H. Reichert, P. Simon, J.-P. Rueff, J. Sottmann, W. Wenzel and A. Grimaud, Understanding Battery Interfaces by Combined Characterization and Simulation Approaches: Challenges and Perspectives, *Adv. Energy Mater.*, 2022, **12**, 2102687.
99 A. Pecoraro, F. Fasulo, M. Pavone and A. B. Muñoz-García, First-principles study of interfacial features and charge dynamics between spiro-MeOTAD and photoactive lead halide perovskites, *Chem. Commun.*, 2023, **59**, 5055–5058.
100 S. P. Ong, V. L. Chevrier, G. Hautier, A. Jain, C. Moore, S. Kim, X. Ma and G. Ceder, Voltage, stability and diffusion barrier differences between sodium-ion and lithium-ion intercalation materials, *Energy Environ. Sci.*, 2011, **4**, 3680.
101 R. Tripathi, S. M. Wood, M. S. Islam and L. F. Nazar, Na-ion mobility in layered Na_2FePO_4F and olivine $Na[Fe,Mn]PO_4$, *Energy Environ. Sci.*, 2013, **6**, 2257.
102 Y. Zheng, P. Zhang, S. Q. Wu, Y. H. Wen, Z. Z. Zhu and Y. Yang, First-Principles Investigations on the Na_2MnPO_4F as a Cathode Material for Na-Ion Batteries, *J. Electrochem. Soc.*, 2013, **160**, A927–A932.
103 S. T. Dacek, W. D. Richards, D. A. Kitchaev and G. Ceder, Structure and Dynamics of Fluorophosphate Na-Ion Battery Cathodes, *Chem. Mater.*, 2016, **28**, 5450–5460.
104 I. L. Matts, S. Dacek, T. K. Pietrzak, R. Malik and G. Ceder, Explaining Performance-Limiting Mechanisms in Fluorophosphate Na-Ion Battery Cathodes through Inactive Transition-Metal Mixing and First-Principles Mobility Calculations, *Chem. Mater.*, 2015, **27**, 6008–6015.
105 T. Yamashita, H. Momida and T. Oguchi, Crystal structure predictions of Na C_6O_6 for sodium-ion batteries: First-principles calculations with an evolutionary algorithm, *Electrochim. Acta*, 2016, **195**, 1–8.
106 Y. Chen, J. Lüder, M.-F. Ng, M. Sullivan and S. Manzhos, Polyaniline and CN-functionalized polyaniline as organic cathodes for lithium and sodium ion batteries: a combined molecular dynamics and density functional tight binding study in solid state, *Phys. Chem. Chem. Phys.*, 2018, **20**, 232–237.
107 Y. Chen and S. Manzhos, A comparative computational study of lithium and sodium insertion into van der Waals and covalent tetracyanoethylene (TCNE)-based crystals as promising materials for organic lithium and sodium ion batteries, *Phys. Chem. Chem. Phys.*, 2016, **18**, 8874–8880.
108 Y. Zhang, R. Zhang and Y. Huang, Air-Stable Na_xTMO_2 Cathodes for Sodium Storage, *Front. Chem.*, 2019, **7**, 335.
109 R. Berthelot, D. Carlier and C. Delmas, Electrochemical investigation of the P2–Na_xCoO_2 phase diagram, *Nat. Mater.*, 2011, **10**, 74–80.
110 N. Yabuuchi and S. Komaba, Recent research progress on iron- and manganese-based positive electrode materials for rechargeable sodium batteries, *Sci. Technol. Adv. Mater.*, 2014, **15**, 043501.
111 M. S. Islam and C. A. J. Fisher, Lithium and sodium battery cathode materials: computational insights into voltage, diffusion and nanostructural properties, *Chem. Soc. Rev.*, 2014, **43**, 185–204.
112 C. Delmas, C. Fouassier and P. Hagenmuller, Structural classification and properties of the layered oxides, *Phys. B + C*, 1980, **99**, 81–85.
113 N. A. Katcho, J. Carrasco, D. Saurel, E. Gonzalo, M. Han, F. Aguesse and T. Rojo, Origins of Bistability and Na Ion Mobility Difference in P2- and O3-$Na_{2/3}Fe_{2/3}Mn_{1/3}O_2$ Cathode Polymorphs, *Adv. Energy Mater.*, 2017, **7**, 1601477.
114 A. Urban, D.-H. Seo and G. Ceder, Computational understanding of Li-ion batteries, *npj Comput. Mater.*, 2016, **2**, 16002.
115 R. J. Clément, P. G. Bruce and C. P. Grey, Review—Manganese-Based P2-Type Transition Metal Oxides as Sodium-Ion Battery Cathode Materials, *J. Electrochem. Soc.*, 2015, **162**, A2589–A2604.
116 C. Zhao, Q. Wang, Z. Yao, J. Wang, B. Sánchez-Lengeling, F. Ding, X. Qi, Y. Lu, X. Bai, B. Li, H. Li, A. Aspuru-Guzik, X. Huang, C. Delmas, M. Wagemaker, L. Chen and Y.-S. Hu, Rational design of layered oxide materials for sodium-ion batteries, *Science*, 2020, **370**, 708–711.

117 X. Zhang, Z. Zhang, S. Yao, A. Chen, X. Zhao and Z. Zhou, An effective method to screen sodium-based layered materials for sodium ion batteries, *npj Comput. Mater.*, 2018, **4**, 13.

118 Q. Wang, S. Mariyappan, G. Rousse, A. V. Morozov, B. Porcheron, R. Dedryvère, J. Wu, W. Yang, L. Zhang, M. Chakir, M. Avdeev, M. Deschamps, Y.-S. Yu, J. Cabana, M.-L. Doublet, A. M. Abakumov and J.-M. Tarascon, Unlocking anionic redox activity in O3-type sodium 3d layered oxides *via* Li substitution, *Nat. Mater.*, 2021, **20**, 353–361.

119 J. Vergnet, M. Saubanère, M.-L. Doublet and J.-M. Tarascon, The Structural Stability of P2-Layered Na-Based Electrodes during Anionic Redox, *Joule*, 2020, **4**, 420–434.

120 R. A. House, U. Maitra, M. A. Pérez-Osorio, J. G. Lozano, L. Jin, J. W. Somerville, L. C. Duda, A. Nag, A. Walters, K. J. Zhou, M. R. Roberts and P. G. Bruce, Superstructure control of first-cycle voltage hysteresis in oxygen-redox cathodes, *Nature*, 2020, **577**, 502–508.

121 M. Ben Yahia, J. Vergnet, M. Saubanère and M.-L. Doublet, Unified picture of anionic redox in Li/Na-ion batteries, *Nat. Mater.*, 2019, **18**, 496–502.

122 C. Zhao, Z. Yao, J. Wang, Y. Lu, X. Bai, A. Aspuru-Guzik, L. Chen and Y.-S. Hu, Ti Substitution Facilitating Oxygen Oxidation in $Na_{2/3}Mg_{1/3}Ti_{1/6}Mn_{1/2}O_2$ Cathode, *Chem*, 2019, **5**, 2913–2925.

123 M. Saubanère, E. McCalla, J. M. Tarascon and M. L. Doublet, The intriguing question of anionic redox in high-energy density cathodes for Li-ion batteries, *Energy Environ. Sci.*, 2016, **9**, 984–991.

124 D.-H. Seo, J. Lee, A. Urban, R. Malik, S. Kang and G. Ceder, The structural and chemical origin of the oxygen redox activity in layered and cation-disordered Li-excess cathode materials, *Nat. Chem.*, 2016, **8**, 692–697.

125 U. Maitra, R. A. House, J. W. Somerville, N. Tapia-Ruiz, J. G. Lozano, N. Guerrini, R. Hao, K. Luo, L. Jin, M. A. Pérez-Osorio, F. Massel, D. M. Pickup, S. Ramos, X. Lu, D. E. McNally, A. V. Chadwick, F. Giustino, T. Schmitt, L. C. Duda, M. R. Roberts and P. G. Bruce, Oxygen redox chemistry without excess alkali-metal ions in $Na_{2/3}[Mg_{0.28}Mn_{0.72}]O_2$, *Nat. Chem.*, 2018, **10**, 288–295.

126 C. Ma, J. Alvarado, J. Xu, R. J. Clément, M. Kodur, W. Tong, C. P. Grey and Y. S. Meng, Exploring Oxygen Activity in the High Energy P2-Type $Na_{0.78}Ni_{0.23}Mn_{0.69}O_2$ Cathode Material for Na-Ion Batteries, *J. Am. Chem. Soc.*, 2017, **139**, 4835–4845.

127 T. Risthaus, D. Zhou, X. Cao, X. He, B. Qiu, J. Wang, L. Zhang, Z. Liu, E. Paillard, G. Schumacher, M. Winter and J. Li, A high-capacity P2 $Na_{2/3}Ni_{1/3}Mn_{2/3}O_2$ cathode material for sodium ion batteries with oxygen activity, *J. Power Sources*, 2018, **395**, 16–24.

128 A. Massaro, A. B. Muñoz-García, P. P. Prosini, C. Gerbaldi and M. Pavone, Unveiling Oxygen Redox Activity in P2-Type $Na_xNi_{0.25}Mn_{0.68}O_2$ High-Energy Cathode for Na-Ion Batteries, *ACS Energy Lett.*, 2021, **6**, 2470–2480.

129 C. Zhao, Z. Yao, Q. Wang, H. Li, J. Wang, M. Liu, S. Ganapathy, Y. Lu, J. Cabana, B. Li, X. Bai, A. Aspuru-Guzik, M. Wagemaker, L. Chen and Y.-S. Hu, Revealing High Na-Content P2-Type Layered Oxides as Advanced Sodium-Ion Cathodes, *J. Am. Chem. Soc.*, 2020, **142**, 5742–5750.

130 M. Sathiya, G. Rousse, K. Ramesha, C. P. Laisa, H. Vezin, M. T. Sougrati, M.-L. Doublet, D. Foix, D. Gonbeau, W. Walker, A. S. Prakash, M. Ben Hassine, L. Dupont and J.-M. Tarascon, Reversible anionic redox chemistry in high-capacity layered-oxide electrodes, *Nat. Mater.*, 2013, **12**, 827–835.

131 J. Hong, W. E. Gent, P. Xiao, K. Lim, D. H. Seo, J. Wu, P. M. Csernica, C. J. Takacs, D. Nordlund, C. J. Sun, K. H. Stone, D. Passarello, W. Yang, D. Prendergast, G. Ceder, M. F. Toney and W. C. Chueh, Metal–oxygen decoordination stabilizes anion redox in Li-rich oxides, *Nat. Mater.*, 2019, **18**, 256–265.

132 E. McCalla, A. M. Abakumov, M. Saubanere, D. Foix, E. J. Berg, G. Rousse, M.-L. Doublet, D. Gonbeau, P. Novak, G. Van Tendeloo, R. Dominko and J.-M. Tarascon, Visualization of O–O peroxo-like dimers in high-capacity layered oxides for Li-ion batteries, *Science*, 2015, **350**, 1516–1521.

133 Y. Zhang, M. Wu, J. Ma, G. Wei, Y. Ling, R. Zhang and Y. Huang, Revisiting the $Na_{2/3}Ni_{1/3}Mn_{2/3}O_2$ Cathode: Oxygen Redox Chemistry and Oxygen Release Suppression, *ACS Cent. Sci.*, 2020, **6**, 232–240.

134 A. Massaro, A. Langella, A. B. Muñoz-García and M. Pavone, First-principles insights on anion redox activity in $Na_xFe_{1/8}Ni_{1/8}Mn_{3/4}O_2$: Toward efficient high-energy cathodes for Na-ion batteries, *J. Am. Ceram. Soc.*, 2023, **106**, 109–119.

135 A. Massaro, A. Langella, C. Gerbaldi, G. Antonio Elia, A. B. Muñoz-García and M. Pavone, Ru-Doping of P2-$Na_xMn_{0.75}Ni_{0.25}O_2$-Layered Oxides for High-Energy Na-Ion Battery Cathodes: First-Principles Insights on Activation and Control of Reversible Oxide Redox Chemistry, *ACS Appl. Energy Mater.*, 2022, **5**, 10721–10730.

136 Q. Shen, Y. Liu, X. Zhao, J. Jin, Y. Wang, S. Li, P. Li, X. Qu and L. Jiao, Transition-Metal Vacancy Manufacturing and Sodium-Site Doping Enable a High-Performance Layered Oxide Cathode through Cationic and Anionic Redox Chemistry, *Adv. Funct. Mater.*, 2021, 2106923.

137 C. J. Cramer, W. B. Tolman, K. H. Theopold and A. L. Rheingold, Variable character of O–O and M-O bonding in side-on (η2) 1:1 metal complexes of O_2, *Proc. Natl. Acad. Sci. U. S. A.*, 2003, **100**, 3635–3640.

138 L. E. Sutton and H. J. M. Bowen, *Tables of Interatomic Distances and Configuration in Molecules and Ions*, The Chemical Society, London, Special edn, 1958.

139 Q. Wang, K. Jiang, Y. Feng, S. Chu, X. Zhang, P. Wang, S. Guo and H. Zhou, P2-Type Layered $Na_{0.75}Ni_{1/3}Ru_{1/6}Mn_{1/2}O_2$ Cathode Material with Excellent Rate Performance for Sodium-Ion Batteries, *ACS Appl. Mater. Interfaces*, 2020, **12**, 39056–39062.

140 N. Kiziltas-Yavuz, A. Bhaskar, D. Dixon, M. Yavuz, K. Nikolowski, L. Lu, R.-A. Eichel and H. Ehrenberg,

Improving the rate capability of high voltage lithium-ion battery cathode material $LiNi_{0.5}Mn_{1.5}O_4$ by ruthenium doping, *J. Power Sources*, 2014, **267**, 533–541.

141 Y. Yu, P. Karayaylali, S. H. Nowak, L. Giordano, M. Gauthier, W. Hong, R. Kou, Q. Li, J. Vinson, T. Kroll, D. Sokaras, C. J. Sun, N. Charles, F. Maglia, R. Jung and Y. Shao-Horn, Revealing Electronic Signatures of Lattice Oxygen Redox in Lithium Ruthenates and Implications for High-Energy Li-Ion Battery Material Designs, *Chem. Mater.*, 2019, **31**, 7864–7876.

142 N. Charles, Y. Yu, L. Giordano, R. Jung, F. Maglia and Y. Shao-Horn, Toward Establishing Electronic and Phononic Signatures of Reversible Lattice Oxygen Oxidation in Lithium Transition Metal Oxides For Li-Ion Batteries, *Chem. Mater.*, 2020, **32**, 5502–5514.

143 B. Mortemard De Boisse, G. Liu, J. Ma, S. I. Nishimura, S. C. Chung, H. Kiuchi, Y. Harada, J. Kikkawa, Y. Kobayashi, M. Okubo and A. Yamada, Intermediate honeycomb ordering to trigger oxygen redox chemistry in layered battery electrode, *Nat. Commun.*, 2016, **7**, 1–9.

144 M. Pavone, A. B. Muñoz-García, A. M. Ritzmann and E. A. Carter, First-principles study of lanthanum strontium manganite: Insights into electronic structure and oxygen vacancy formation, *J. Phys. Chem. C*, 2014, **118**, 13346–13356.

145 A. M. Ritzmann, A. B. Muñoz-García, M. Pavone, J. A. Keith and E. A. Carter, Ab Initio DFT+*U* Analysis of Oxygen Vacancy Formation and Migration in $La_{1-x}Sr_xFeO_{3-\delta}$ (x = 0, 0.25, 0.50), *Chem. Mater.*, 2013, **25**, 3011–3019.

146 P. Yan, J. Zheng, Z.-K. Tang, A. Devaraj, G. Chen, K. Amine, J.-G. Zhang, L.-M. Liu and C. Wang, Injection of oxygen vacancies in the bulk lattice of layered cathodes, *Nat. Nanotechnol.*, 2019, **14**, 602–608.

147 Y. Xie, Y. Jin and L. Xiang, Li-rich layered oxides: Structure, capacity and voltage fading mechanisms and solving strategies, *Particuology*, 2022, **61**, 1–10.

148 C. Delmas, D. Carlier and M. Guignard, The Layered Oxides in Lithium and Sodium-Ion Batteries: A Solid-State Chemistry Approach, *Adv. Energy Mater.*, 2021, **11**, 2001201.

149 M. G. T. Nathan, H. Yu, G. Kim, J. Kim, J. S. Cho, J. Kim and J.-K. Kim, Recent Advances in Layered Metal-Oxide Cathodes for Application in Potassium-Ion Batteries, *Adv. Sci.*, 2022, **9**, 2105882.

150 N. Voronina, M.-Y. Shin, H. Kim, N. Yaqoob, O. Guillon, S. H. Song, H. Kim, H.-D. Lim, H.-G. Jung, Y. Kim, H. Lee, K.-S. Lee, K. Yazawa, K. Gotoh, P. Kaghazchi and S.-T. Myung, Hysteresis-Suppressed Reversible Oxygen-Redox Cathodes for Sodium-Ion Batteries, *Adv. Energy Mater.*, 2022, **12**, 2103939.

151 L. Yang, R. Chen, Z. Liu, Y. Gao, X. Wang, Z. Wang and L. Chen, Configuration-dependent anionic redox in cathode materials, *Battery Energy*, 2022, **1**, 20210015.

152 X.-L. Li, C. Ma and Y.-N. Zhou, Transition Metal Vacancy in Layered Cathode Materials for Sodium-Ion Batteries, *Chem. – Eur. J.*, 2023, **29**, e202203586.

153 J. Feng, S. Luo, M. Sun, J. Cong, S. Yan, Q. Wang, Y. Zhang, X. Liu, W. Mu and P. Hou, Investigation of Ti-substitution and $MnPO_4$ coating effects on structural and electrochemical properties of P2-$Na_{0.67}Ti_xNi_{0.33}Mn_{0.67-x}O_2$ cathode materials, *Appl. Surf. Sci.*, 2022, **600**, 154147.

154 J. Feng, S. Luo, J. Cong, K. Li, S. Yan, Q. Wang, Y. Zhang, X. Liu, X. Lei and P. Hou, Synthesis and electrochemical properties of Co-free P2/O3 biphasic $Na_{1-x}Li_xNi_{0.33}Mn_{0.67}O_2$ cathode material for sodium-ion batteries, *J. Electroanal. Chem.*, 2022, **916**, 116378.

155 G. Ponti, F. Palombi, D. Abate, F. Ambrosino, G. Aprea, T. Bastianelli, F. Beone, R. Bertini, G. Bracco, M. Caporicci, B. Calosso, M. Chinnici, A. Colavincenzo, A. Cucurullo, P. Dangelo, M. De Rosa, P. De Michele, A. Funel, G. Furini, D. Giammattei, S. Giusepponi, R. Guadagni, G. Guarnieri, A. Italiano, S. Magagnino, A. Mariano, G. Mencuccini, C. Mercuri, S. Migliori, P. Ornelli, S. Pecoraro, A. Perozziello, S. Pierattini, S. Podda, F. Poggi, A. Quintiliani, A. Rocchi, C. Scio, F. Simoni and A. Vita, in *2014 International Conference on High Performance Computing & Simulation (HPCS)*, IEEE, 2014, pp. 1030–1033.